



LUND UNIVERSITY

Kinetic and thermodynamic modelling of ternary nanowire growth

Leshchenko, Egor

2021

Document Version:

Publisher's PDF, also known as Version of record

[Link to publication](#)

Citation for published version (APA):

Leshchenko, E. (2021). *Kinetic and thermodynamic modelling of ternary nanowire growth*. [Doctoral Thesis (compilation), Lund University]. Solid State Physics, Lund University.

Total number of authors:

1

Creative Commons License:

Unspecified

General rights

Unless other specific re-use rights are stated the following general rights apply:

Copyright and moral rights for the publications made accessible in the public portal are retained by the authors and/or other copyright owners and it is a condition of accessing publications that users recognise and abide by the legal requirements associated with these rights.

- Users may download and print one copy of any publication from the public portal for the purpose of private study or research.
- You may not further distribute the material or use it for any profit-making activity or commercial gain
- You may freely distribute the URL identifying the publication in the public portal

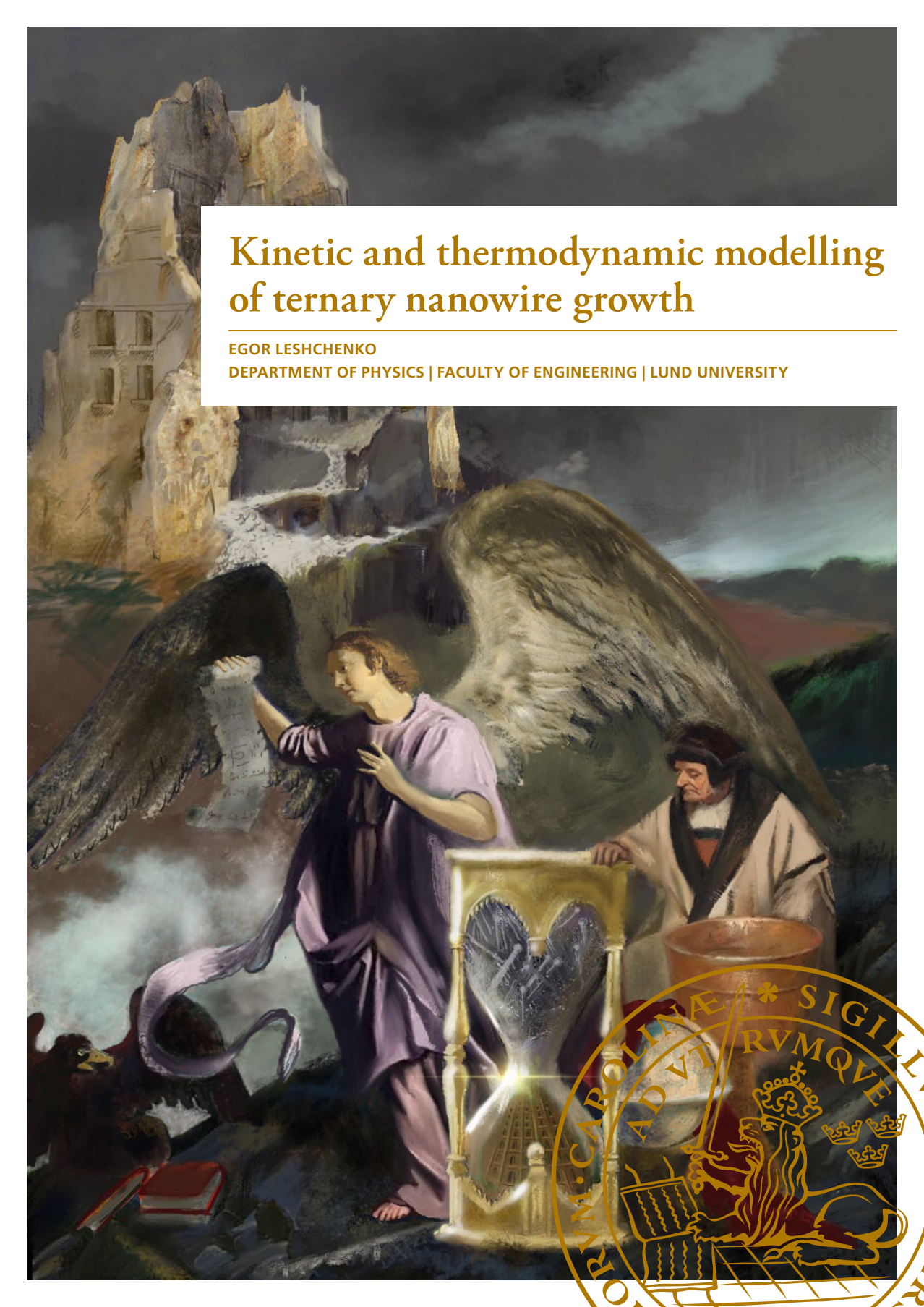
Read more about Creative commons licenses: <https://creativecommons.org/licenses/>

Take down policy

If you believe that this document breaches copyright please contact us providing details, and we will remove access to the work immediately and investigate your claim.

LUND UNIVERSITY

PO Box 117
221 00 Lund
+46 46-222 00 00



Kinetic and thermodynamic modelling of ternary nanowire growth

EGOR LESHCHENKO

DEPARTMENT OF PHYSICS | FACULTY OF ENGINEERING | LUND UNIVERSITY





Lund University
Faculty of Engineering
Department of Physics

ISBN 978-91-8039-006-4



Kinetic and thermodynamic modelling of ternary nanowire growth

Kinetic and thermodynamic modelling of ternary nanowire growth

Egor Leshchenko



LUND
UNIVERSITY

DOCTORAL DISSERTATION

by due permission of the Faculty of Engineering, Lund University, Sweden.
Will be publicly defended on Friday October 29th 2021 at 9:15 in Rydbergsalen at
the Department of Physics, Sölvegatan 14, Lund, Sweden for the degree of
Doctor of Philosophy in Engineering

Faculty opponent

Prof. Faustino Martelli

Institute of Microelectronics and Microsystems, Italy

Organization LUND UNIVERSITY Division of Solid State Physics Department of Physics P.O. Box 118, SE-221 00 Lund, Sweden Author: Egor Leshchenko		Document name DOCTORAL DISSERTATION
		Date of disputation 2021-10-29
		Sponsoring organization
Title and subtitle Kinetic and thermodynamic modelling of ternary nanowire growth		
Abstract Among nanoscale structures of different shapes and dimensions nanowires are one of the most promising because of its truly unique properties different from their bulk counterparts. The energy quantization, perfect defect-free structure, and the possibility to grow them within the miscibility gap in combination with the benefits of bottom-up design and the possibility of integration on silicon substrates make nanowires ideal candidates for applications in optoelectronics, biotechnology and energy harvesting. Today the research focus shifts toward the investigation of more complex materials, namely ternary and quaternary nanowires. For the majority of applications, a critical step in the nanowire-based device design is the ability to control the composition and crystal structure of ternary III-V nanowires. Such tuning is impossible without understanding of the underlying growth mechanism. Theoretical modelling may provide insight into the growth processes and help to assess optimal growth conditions. Moreover, simulation of nanowire growth allows one to reduce the number of experiments, which is essential in view of its high cost. In this perspective, a set of models that encompass a variety of aspects of ternary nanowire formation including their composition and crystal structure has been developed. Within the modelling both thermodynamic and kinetic approaches have been used. The first model is based on two-component nucleation theory and describes the formation of the critical nucleus from a quaternary liquid. An analytic expression that links the compositions of the ternary nucleus and liquid particle is derived. The nucleus composition of four materials systems is discussed in details. Next, we explain how the surface energy influences the miscibility gap and the liquid-solid composition dependence during nucleation from a liquid melt. The second model is based on the consideration of the incorporation rates of binary species into the monolayer and describes the evolution of the solid composition from the nucleated-limited composition to the kinetic one. The kinetic steady state regime is used to fit an experimental data set, namely the liquid-solid composition dependence obtained during growth of $\text{In}_x\text{Ga}_{1-x}\text{As}$ nanowires in an environmental transmission electron microscope. Finally, a model which describes the composition dependence of the zinc blende – wurtzite polytypism in ternary nanowires growing by the vapor-liquid-solid mechanism is developed.		
Key words III-V semiconductor materials, ternary nanowires, composition, crystal structure, modelling		
Classification system and/or index terms (if any)		
Supplementary bibliographical information		Language English
ISSN and key title		ISBN 978-91-8039-006-4 (print) 978-91-8039-007-1 (pdf)
Recipient's notes	Number of pages 168	Price
	Security classification	

I, the undersigned, being the copyright owner of the abstract of the above-mentioned dissertation, hereby grant to all reference sources permission to publish and disseminate the abstract of the above-mentioned dissertation.

Signature



Date 2021-09-20

Kinetic and thermodynamic modelling of ternary nanowire growth

Egor Leshchenko



LUND
UNIVERSITY

Cover illustration: As can be seen from the title, this thesis covers several topics. The two most important keywords are modelling and nanowires. This combination and my love for art sparked an idea for the creation of this image. As is often the case with art, the painting can be interpreted in many ways. Thus, I would prefer not to explain the symbols and meanings built in the image leaving its interpretation to the reader. As for me, only for the Tower I see three interpretations at different “scales”: personal, “making a theory” and “science and progress” levels. Or, maybe, someone can remember the story about Richard Feynman and the interdisciplinary conference... The cover art is inspired by the Northern Renaissance and drawn by Russian painter, Boris A. Tarasov. One can find references to and echoes of 16th and 17th century painters.

© Egor Leshchenko

Copyright pp i – xvi and 1 – 69, Egor Leshchenko 2021

Paper 1 © The Royal Society of Chemistry 2018

Paper 2 © The Royal Society of Chemistry 2021

Paper 3 © MDPI 2020

Paper 4 © American Chemical Society 2021

Paper 5 © Elsevier B.V. 2019

Division of Solid State Physics, Department of Physics
Faculty of Engineering, Lund University

ISBN 978-91-8039-006-4 (print)

ISBN 978-91-8039-007-1 (pdf)

Printed in Sweden by Media-Tryck, Lund University Lund 2021



Media-Tryck is a Nordic Swan Ecolabel
certified provider of printed material.
Read more about our environmental
work at www.mediatryck.lu.se

MADE IN SWEDEN 

*Travelling is quite useful, it makes your imagination work.
Everything else is deception and tiredness. Our own trip is
entirely imaginary, here is its strength.*

Louis Ferdinand Celine
“Journey to the End of the Night”

Contents

Abstract	iii
Popular Science Summary	v
List of Papers	ix
List of Abbreviations and Notations	xi
Acknowledgments	xv
1 Introduction	1
1.1 Growth methods of nanowires	3
1.2 Modelling strategies for nanowire growth	6
1.3 Thesis outline	10
2 Fundamentals of Nucleation Theory	11
2.1 Thermodynamics of phase transition	11
2.2 Gibbs energy of substitutional solution phases	13
2.3 Formation energy	16
2.4 Chemical potentials in multicomponent systems	18
2.5 Miscibility gap	19
2.6 Surface energy	21
3 Vapor-Liquid-Solid Growth of Nanowires	23
3.1 Vapor–liquid–solid mechanism	23
3.2 Ternary nanowires	27
3.3 Nanowire composition	28
3.3.1 Equilibrium model	30
3.3.2 Nucleation model	31
3.3.3 Incorporation model	34
3.3.4 Material balance model	36
3.4 Nanowire crystal structure	39

4 Nanowire Growth Modelling and Results	41
4.1 Assumptions and limitations	41
4.2 Composition of ternary nanowires	43
4.2.1 Nucleation-limited composition	44
4.2.2 Incorporation-limited composition	51
4.2.3 Comparison theory and <i>in-situ</i> analysis.....	53
4.3 Crystal structure of InGaAs nanowires	54
5 Summary and Outlook.....	57
References	61

Abstract

Among nanoscale structures of different shapes and dimensions nanowires are one of the most promising because of its truly unique properties different from their bulk counterparts. The energy quantization, perfect defect-free structure, and the possibility to grow them within the miscibility gap in combination with the benefits of bottom-up design and the possibility of integration on silicon substrates make nanowires ideal candidates for applications in optoelectronics, biotechnology and energy harvesting. Today the research focus shifts toward the investigation of more complex materials, namely ternary and quaternary nanowires. For the majority of applications, a critical step in the nanowire-based device design is the ability to control the composition and crystal structure of ternary III-V nanowires. Such tuning is impossible without understanding of the underlying growth mechanism. Theoretical modelling may provide insight into the growth processes and help to assess optimal growth conditions. Moreover, simulation of nanowire growth allows one to reduce the number of experiments, which is essential in view of its high cost.

In this perspective, a set of models that encompass a variety of aspects of ternary nanowire formation including their composition and crystal structure has been developed. Within the modelling both thermodynamic and kinetic approaches have been used.

The first model is based on two-component nucleation theory and describes the formation of the critical nucleus from a quaternary liquid. An analytic expression that links the compositions of the ternary nucleus and liquid particle is derived. The nucleus composition of four materials systems is discussed in details. Next, we explain how the surface energy influences the miscibility gap and the liquid-solid composition dependence during nucleation from a liquid melt.

The second model is based on the consideration of the incorporation rates of binary species into the monolayer and describes the evolution of the solid composition from the nucleated-limited composition to the kinetic one. The kinetic steady state regime is used to fit an experimental data set, namely the liquid-solid composition dependence obtained during growth of $\text{In}_x\text{Ga}_{1-x}\text{As}$ nanowires in an environmental transmission electron microscope.

Finally, a model which describes the composition dependence of the zinc blende – wurtzite polytypism in ternary nanowires growing by the vapor-liquid-solid mechanism is developed.

Popular Science Summary

In a rapidly globalizing world, the progress and success in the electronics industry are inextricably linked to the miniaturization of electronics. The smaller the size of an electronic device, the more such devices can be fit into the same area. For example, the current type of transistor, invented in 1947, was 40 micrometers long, while IBM announced in May 2021 a chip with 2 nanometer transistors. The difference in the length scale is 20000 times (the same as the difference between the length of a Pharaoh ant and an African bush elephant). Somewhere in between, humanity made a step into the nanoscale world. The prefix “nano” comes from ancient Greek for “dwarf” and denotes $1/1\ 000\ 000\ 000$, or one billionth.

In addition to a higher packing density of the electronic chips, which results in higher performance and lower energy use, the transition to nanoscale enables the materials to exhibit unique properties directly connected to its small size. When the size is small enough, that is on the nanometer scale, quantum mechanical effects start to dominate and one such effect is that the motion of electrons get restricted and this is known as quantum confinement. Considering the size, there are three main types of nanostructures, namely 0-dimensional with quantum confinement in all three spatial directions, 1-dimensional, with quantum confinement in two directions, and 2-dimensional with quantum confinement in one direction. The 0-dimensional nanostructures are known as quantum dots, the 1-dimensional ones as quantum wires or nanowires, and the 2-dimensional ones as quantum wells. Even if nanostructures cannot be seen with the naked eyes, their influence is more and more perceptible: they incorporate into our daily life and change it. For example, a regular customer can buy a high-resolution TV with quantum dots or glossy printing paper with ceramic nanoparticles.

Among the nanostructures of different shapes and dimensions, the nanowires are of particular interest and importance. They are whisker-like crystals with the radius of 10-100 nanometers and the length of a few micrometers. Despite there are no nanowire-based devices in today’s industry, many prototypes have been developed such as solar cells, sensors, transistors, light emitting diodes and silicon nanowire-based batteries announced by Tesla. Such a variety of applications can be explained by the possibility of controlled growth of nanowires, including their morphology (the radius and length), chemical composition (sort and number of atoms which form a nanowire) and crystal structure (the arrangement of the atoms in the crystal). This allows one to tune the optical and electrical properties of nanowires. For

example, combining two binary compounds, such as indium arsenide (InAs) and gallium arsenide (GaAs), one may obtain ternary InGaAs nanowires whose properties are a combination of those of the binary compounds (InAs and GaAs). To be more specific, the properties of ternary nanowires are determined by the ratio of the number of the InAs and GaAs units in the solid. In this perspective, an important question arises: how to make a nanowire with a given chemical composition?

To answer this question, we should understand the underlying growth mechanism and know how to control the process using experimental conditions such as temperature and fluxes. The most popular way to fabricate nanowires is by so called vapor-liquid-solid growth. Within this approach, the fluxes of atomic species are directed towards a sample surface containing liquid metal droplets. Then, atoms dissolve into the liquid droplets, and when the concentration of atoms exceeds the solubility limit, it is energetically favourable for crystalline material to form. This formation process takes place at the contact area between the sample surface and the liquid drop. Continuing this process, a nanowire takes form, one atomic layer after another, until the fluxes of atomic species from the vapor are turned off.

Now, when we understand the principle behind nanowire formation, we would like to know how the composition of the liquid drop is related to the composition of the vapor, and how the composition of the solid nanowire is related to the liquid. If we know this, we can predict, on average, which atom, red or white (see Figure 1), will incorporate into the nanowire depending on the conditions.

One of the purposes of this thesis is to find the relationships between these compositions using a variety of models, which are based on different assumptions and limiting steps. Another purpose is to explain the crystal structure of ternary nanowires. The research procedure is the following. When considering nanowire growth, I assume the most critical elementary processes, which I translate into equations. Then I solve these equations and analyse their solutions under the variation of different, experimentally relevant parameters, such as concentrations and nanowire growth temperature.

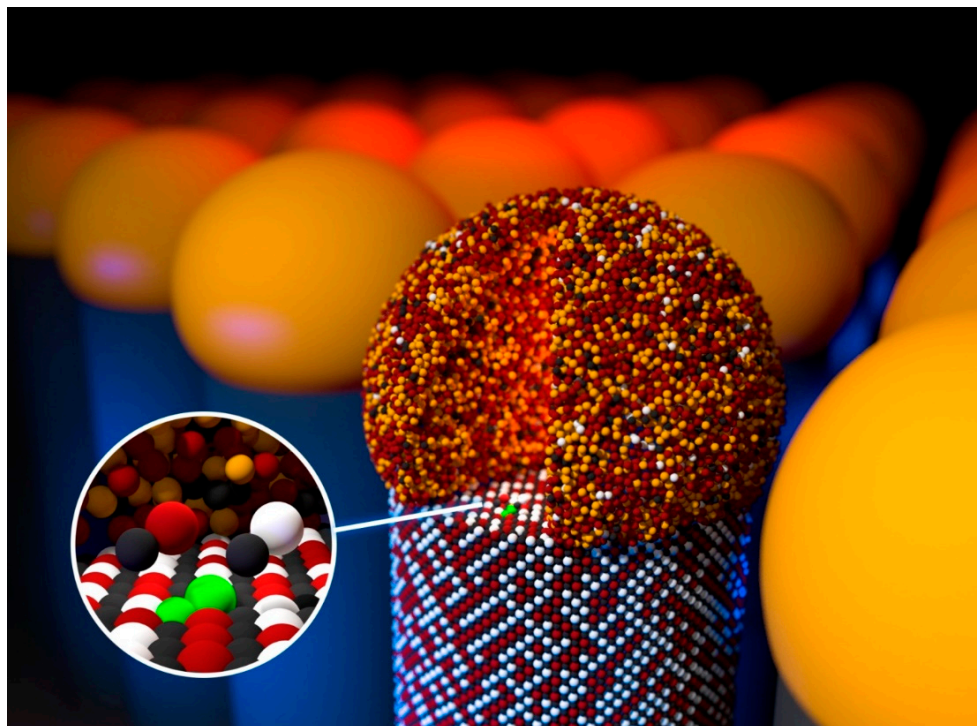


Figure 1. Schematic illustration of a ternary nanowire array. The structure in the “focus” is a nanowire and the droplet situated on the nanowire tip. Both of them are built by a large number of the small spheres, which denote atoms. Their colour corresponds to one of the sorts of atoms. For example, the nanowire is made of three sorts of atoms, namely indium (red spheres), gallium (white spheres) and arsenic (black spheres). As discussed earlier, a ternary nanowire can be considered as a combination of binary compounds, or the atom pairs (InAs and GaAs). The droplet consists of four sorts of atoms. The fourth component (yellow spheres) is gold, which serves as a solvent. The atoms in the crystal are well arranged, while the atoms in the droplet are randomly distributed. A piece of the droplet is cut for illustrative purpose. The main question, shown in the inset, is, ‘which pair of atoms (InAs or GaAs) should be instead of the “unknown” green pair’? Reprinted with permission from The Royal Society of Chemistry 2018 (Paper I).

List of Papers

This doctoral thesis is based on the following articles:

I. Nucleation-limited composition of ternary III-V nanowires forming from quaternary gold based liquid alloys

Egor D. Leshchenko, Masoomeh Ghasemi, Vladimir G. Dubrovskii and Jonas Johansson.

CrystEngComm, 2018, 20, 1649 – 1655.

I developed the model together with J.J. and V.D., namely I considered the most general case of the composition-dependent pseudo-binary interaction parameter. I performed the calculations for two of four material systems. With the exception of the model part, I wrote the paper.

II. Surface energy driven miscibility gap suppression during nucleation of III-V ternary alloys

Egor D. Leshchenko and Jonas Johansson.

CrystEngComm, 2021, 23, 5284 – 5292.

I developed the model with advice from J.J. I performed the calculations. I wrote the paper.

III. Role of thermodynamics and kinetics in the composition of ternary III-V nanowires

Egor D. Leshchenko and Jonas Johansson.

Nanomaterials, 2020, 10, 2553.

I developed the model with advice from J.J. I performed the calculations. I wrote the paper.

IV. Compositional correlation between the nanoparticle and the growing Au-assisted In_xGa_{1-x}As nanowires

Robin Sjökvist, Daniel Jacobsson, Marcus Tornberg, Reine Wallenberg, Egor D. Leshchenko, Jonas Johansson, Kimberly A. Dick
Journal of Physical Chemistry Letters, 2021, 12, 31, 7590 – 7595.

I developed the model and performed the model calculations with advice from J.J. R.S. carried out the experiments supported by D.J., M.T., R.W, and K.A.D.

V. Zinc blende and wurtzite crystal structure formation in gold catalyzed InGaAs nanowires

Jonas Johansson and Egor D. Leshchenko.

Journal of Crystal Growth, 2019, 509, 118 – 123.

I developed the model together with J.J. I performed the calculations. I wrote the introduction and results and discussion parts.

The following articles are not included in this thesis; however, they are related to the topic of this thesis:

VI. Assembling your nanowire: an overview of composition tuning in ternary III–V nanowires

Masoomah Ghasemi, Egor D. Leshchenko and Jonas Johansson.

Nanotechnology, 2020, 32, 072001.

VII. Tuning the morphology of self-assisted GaP nanowires

Egor D. Leshchenko, Paul Kuyanov, Ray Lapierre and Vladimir G. Dubrovskii

Nanotechnology, 2018, 29, 225603.

List of Abbreviations and Notations

Symbols

W^+	attachment rate
W^-	detachment rate
E_i^g	band gap
k_B	Boltzmann constant
ΔS	change of drop surface
μ_i	chemical potential
c_i	concentration (in the liquid)
β	contact angle
χ_i	coefficient which describes the beam geometry in MBE and the cracking efficiency in MOVPE
χ	fraction of the edge length of the nucleus which is not in contact with the vapor phase
λ_i	diffusion length
Γ	effective surface energy (see eq. (28))
a	effective surface energy (see eq. (34))
S	entropy
I^i	flux
R	gas constant
G	Gibbs free energy
F	formation energy
ω_i	(binary or ternary) interaction parameter
ω_s	pseudo-binary interaction parameter
a_i	lattice parameter

h	layer height
y	liquid composition, $y = c_A/(c_A + c_B)$
γ_i	surface energy
x_i	mole fraction of component i
R_{NW}	nanowire radius
s	number of III-V pairs in the nucleus (nucleus size)
N_i	number of AD (or BD) pairs in the solid
N	number of components
n_i	particle number of species i
P_n	nucleus perimeter
P	pressure
ζ	supersaturation
x	solid composition
T	temperature
V	volume
Ω^i	volume per III-V pair

There are a few more locally used symbols whose definitions are given once they are introduced.

Abbreviations

CALPHAD	calculation of phase diagrams
HVPE	hydride vapor-phase epitaxy
MBE	molecular beam epitaxy
MOVPE	metal organic vapor phase epitaxy
NW	nanowire
VLS	vapor-liquid-solid
VSS	vapor-solid-solid
SLS	solution-liquid-solid
SSS	solution-solid-solid

SFLS	supercritical fluid–liquid–solid
EBL	electron beam lithography
NIL	nanoimprint lithography
SAE	selective area epitaxy
2D	2-dimensional
TPL	triple phase line
C	central
WZ	wurtzite
ZB	zinc blende
<i>V</i>	vapor
<i>L</i>	liquid
<i>S</i>	solid
<i>N</i>	nucleus
<i>o</i>	refers to the pure component
<i>E</i>	excess
<i>dir</i>	direct impingement
<i>re</i>	re-emission
<i>des</i>	desorption
<i>bin</i>	binary (interactions)
<i>ter</i>	ternary (interactions)
<i>high</i>	high order (starting from quaternary interactions)
<i>b</i>	binodal
<i>sp</i>	spinodal
*	refers to the critical nucleus
<i>kin</i>	kinetic
<i>e</i>	equilibrium

Acknowledgments

First and foremost, I would like to thank my supervisor, Jonas Johansson for being the Ariadne's thread helping me to find a path through the labyrinth of theoretical physics. You inspire me to move forward and to develop new ideas. You showed me that one can do science to have fun.

I am indebted to my previous supervisor, Vladimir G. Dubrovskii. I feel truly privileged to have learned from you and not only scientifically.

I thank my co-supervisor Martin Magnusson for nice discussions. I appreciate all your advices, whether they are related to science or not!

Funding for this project came from European Commission within INDEED network under the H2020 program. Due to your financial support, 15 early-stage researchers from around the globe got the opportunity to study and work in the outstanding universities and companies. Natalia, I cannot imagine the project without your coordination. Ridvan, Alejandro, Wonjong, Aswathi, Timur, Sabbir, Anton, Nemanja, Vasili, Pablo, Manuel, Nuño, Michal, Ehsan and Rodion, that was amazing!

I cannot enough emphasize the value of the help in learning CALPHAD that I received from Masoomah Ghasemi. My full gratitude goes out to my colleagues from International research laboratory of physics of epitaxial nanostructures, namely Nickolay, Yury and Alexander.

I am extremely thankful to my numerous co-authors with whom I was lucky to collaborate. Among others, I thank Ray LaPierre, Teemu Hakkarainen, Elisabetta Maria Fiordaliso, Kimberly A. Dick and Robin Sjökvist for fruitful discussions.

My thanks also go to Frank Glas and Federico Panciera for the internship at C2N (Paris, France) where I worked on the nucleation statistics. Among other things, this trip gave me the opportunity to experience the French culture.

I am grateful to artists who drawn cover arts for my papers and thesis. They are Lev Tagin (the cover art “Nanowire-kulich”) and Boris A. Tarasov (the cover art “David and Goliath” and the cover image for this thesis). “Kulich” is a Russian kind of Easter bread.

I have been honoured over the past four years to live among all the friendly people at Solid State Physics. I acknowledge the support and resources from NanoLund. An extra thank you to my lecturers who taught me.

Special thank goes to Lukas, my office mate, who has become a good friend. Thank you for tolerating me for all this time.

Finally, I would like to thank my family and closest friends for their support and guidance over these years.

Egor Leshchenko
Lund University
2021

1 Introduction

After a tremendous number of scientists from different fields dived into the nanoscale world, nanoobjects of various shapes and dimensions began to appear on the pages of scientific journals. Strictly speaking, there is some discrepancy in the definition of nanostructures. One may refer to its size. For example, according to the International Union of Pure and Applied Chemistry, the upper limit for the size of nanoparticles is 100 nanometers of any shape. Nowadays, the prefix “nano” with respect to the structures is often attributed to those which exhibit quantum-size effects. From this perspective, remembering the situation in evolutionary biology with the blurred boundaries of the appearance of a new class or family of animals, it is hard to tell the exact date which marks the first fabrication of nanowires. For example, should we consider whiskers synthesized by Wagner and Ellis in 1964 [1] as an “ancestor” of nanowires or as the first nanowires?

After the discovery of whiskers in 1960s (called so due to their whisker-like morphology, namely the high length to diameter ratio), these structures were almost abandoned. Among important milestones, one may highlight the concept of quantum wires by H. Sakaki [2] and the investigations by E. I. Givargizov [3].

Nanowires earned their place in the spotlight at the dawn of the 21st century with its study by the research groups of C. M. Lieber (Harvard University, USA), L. Samuelson (Lund University, Sweden), and P. Yang (UC Berkeley, USA). A huge number of papers on nanowire growth from scientists indicates the great interest in this field (see Figure 1.1). As seen, the number of nanowire-related papers has reached a plateau and its fate depends on industrial applications.

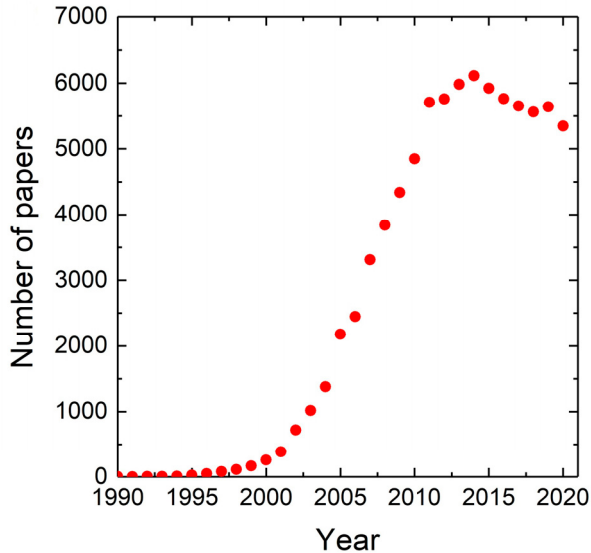


Figure 1.1. Number of nanowire-related papers versus year taken from Scopus (by searching with the keyword “nanowire”).

Such research interest is inextricably linked to various properties offered by nanowires, such as self-assembly, integration with silicon substrates, the possibility of growth of non-planar heterostructures and opportunities to control their morphology, chemical composition, optical and electronic properties. However, there is a gap between academia and industry. Despite a number of prototypes of nanowire-based devices such as solar cells [4], photodetectors [5], biosensors [6], and transistors [7], there are not yet any commercial applications. Like in other fields of nanotechnology, the profitability of the production of such devices is limited by the “Triangle of death” defined by the throughput, quality and cost. Ideally, either a nanowire fabrication technology should be simple and cheap, or the device should be unique and much demanded ensuring a high selling price.

For a long time, nanowire growth has been comparable to a “black box”: all the important measurements were made *ex-situ*, i.e. after growth when the droplet situated on the nanowire tip had solidified. Obviously, with this kind of experiments some information is lost, especially the chemical composition of the liquid particle during growth. However, this did not prevent scientists from making suggestions and theories. Indeed, one can go even further. Lev Landau, the soviet scientist, being very impressed by the Theory of relativity said «the greatest triumph of the power of human genius is that a person is able to understand things that he is no longer able to imagine».

Only recently, with the development of *in-situ* techniques, which combine transmission electron microscopy with the nanowire growth chamber, scientists have managed to get insight into the process of nanowire growth in real time. This has led to a series of research studies on synthesis of binary III-V nanowires in a transmission electron microscope by F. Ross [8], J.-C. Harmand [9] and D. Jacobsson [10]. Thus, today there is a possibility to verify the compliance of the developed theories with the growth process.

This thesis is mainly devoted to theoretical studies. Its hearth is nucleation theory with all its strengths and weaknesses. One of the main purposes is to find the relationship between the chemical composition of Au- and self-catalyzed nanowires and the composition of the liquid catalyst, or seed particle. Taking in mind that experiments on nanowire growth are relatively expensive and time-consuming, the main intention of this thesis is to explain some of the aspects of the nanowire formation, which, I hope, will help to optimize growth conditions.

1.1 Growth methods of nanowires

Starting the consideration of nanowire growth, it makes sense to compare it with the building process. In both nano- and macro-processes there are two completely opposite approaches to “build” something. As for building, the first one is rock-cut architecture with the impressive example of Kailasa temple (Ellora, India), which has been created by carving it out of solid natural rock. The second one is the conventional architecture with the most illustrative example of the Pyramid of Cheops (Giza, Egypt) consisting of almost identical limestone and granite blocks. In the nanoscale world, they correspond to the top-down and bottom-up approaches, which employ etching by chemicals instead of chisels and hammers and atoms as building blocks, respectively.

Trying to find a flexible, well-controlled, and fast growth technology, different methods and techniques for nanowire fabrication have been developed within both approaches. They are summarized and schematically presented in Figure 1.2.

Top-down approach is a subtractive process within which both planar and free-standing nanowires can be obtained as a result of dry etch of the semiconductor substrate with the masking patterns on the top. For surface patterning, one may use *electron beam lithography* (EBL) [11], *nanoimprint lithography* (NIL) [12] and other methods followed by development of a resist layer. Then the pattern is transferred into the semiconductor wafer. Despite high resolution of the patterns which could be achieved ($\sim 2 - 5$ nanometers) [13], this is an expensive and very slow process.

Bottom-up approach for nanowire fabrication being an additive process, involves self-assembly of atoms, which incorporate one-by-one into a cluster producing a nanostructure, which consists thousands of atoms.

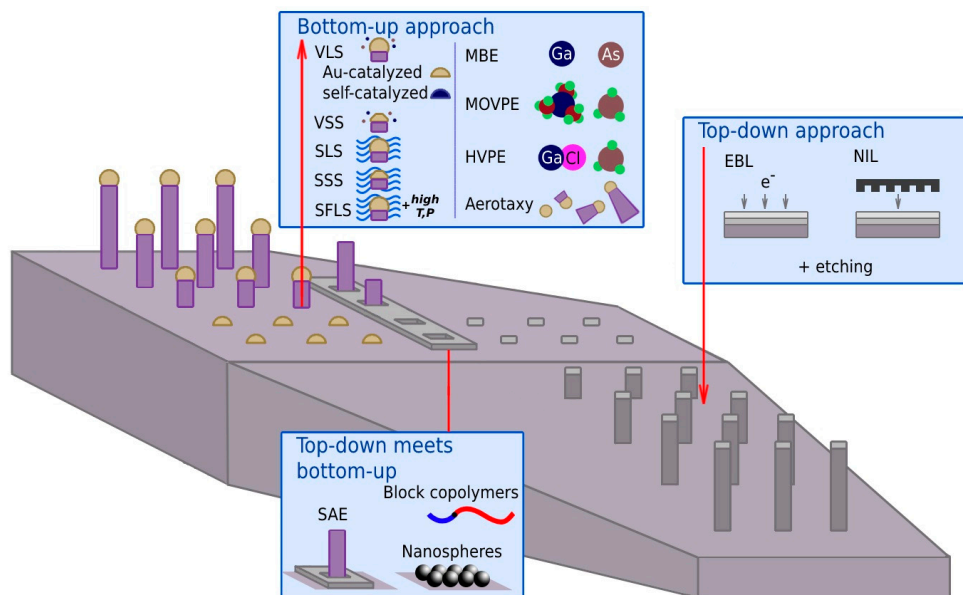


Figure 1.2. Schematic illustration of methods of nanowire growth.

Considering the nanowire formation mechanism, namely the sequence of phase boundary crossings of atoms, one may classify nanowire growth as follows:

Vapour-liquid-solid growth (VLS) [14], [15]. Within this mechanism, atoms feed a liquid particle from the ambient vapor leading to vertical crystal growth as a result of nucleation and monolayer completion, which follows continuously in a quasi-periodic manner. This growth mechanism was first reported by Wagner and Ellis in 1964 [1]. Within their experiments, SiCl_4 molecules were deposited on a Si substrate with gold droplets. A relatively large concentration of Si leads to a supersaturation resulting in nucleation and growth. The growth occurs under the gold droplets only (ignoring possible parasitic growth). This way of formation is known as the VLS mechanism due to the three phases involved in the growth. These droplets play the role of collection sites of semiconductor materials (Si atoms). This is the so-called *Au-catalyzed growth* [16], or more generally, growth with a foreign catalyst.

Afterwards, the research interest has been shifted to usage of group III elements as catalysts instead of a foreign metal catalyst, such as Au, allowing the avoidance of nanowire contamination and degradation of their optoelectronic properties [17]. This growth method called *self-catalyzed growth* became a real breakthrough [18],

[19]. So, self-catalyzed growth goes beyond foreign metal catalyzed growth in morphology control of nanowires due to the self-focusing effect [20], [21], [22]. The effect is that nanowire radii converge to a certain radius during growth because of different radius dependence of atomic fluxes. Thus, the self-focusing effect enables the growth of a nanowire array with a high degree of uniformity of the nanowire diameters despite of the initial droplet size distribution. That is in contradiction to foreign metal catalyzed growth where the nanowire radius is predominantly determined by the radius of the foreign metal catalyst droplet.

Vapor-solid-solid growth (VSS) [23]. It involves the incorporation of atoms into the crystalline solid-metal catalyst particle from the vapor phase and solid-phase diffusion towards the particle-nanowire interface. A clear evidence of such mechanism is that growth occurs at temperatures below the eutectic temperature. On the other hand, temperature should be relatively high to ensure the high rate of solid-phase diffusion.

In addition to these two mechanisms, there are less common formation mechanisms when the vapor phase is replaced by a solution. Depending on the phase of the metallic nanoparticles which could be in the molten or in the solid form, they are *solution-liquid-solid* (SLS) [24], [25] and *solution-solid-solid* (SSS) [26], [27] growth, respectively. Finally, one distinguishes *supercritical fluid-liquid-solid* (SFSL) [28] growth conducted at temperatures and pressures that exceed the critical point of the solvent.

Next, based on the growth machines and precursor types and its delivery route, one can identify the following types of epitaxy:

Molecular beam epitaxy (MBE) was developed in the late 1970s by J.R. Arthur and A.Y. Cho and is one of the most popular and advanced growth techniques [19], [29]. This process consists of deposition of semiconductor materials in ultra-high vacuum conditions with beams of atoms or molecules. The MBE process is characterized by an absence of homogeneous reactions in the growth chamber and high control of growth parameters such as purity of sources, precise flux ratio, and a quick beam flux switch, which is not available for other techniques. This results in abrupt interfaces, high degree of crystallinity and high uniformity of nanowire arrays. The precise control and a relatively low growth rate make this method the best for growth of nanowire-based heterostructures which are required for fabrication of solar cells, lasers and single photon sources. The negative aspect is the complexity and high cost of growth equipment and service (semiconductor sources and substrates).

Metal organic vapor phase epitaxy (MOVPE) [30] is another epitaxial technique widely used to grow nanowires. The MOVPE growth process involves the pyrolysis of organometallic precursor molecules, which makes the chemistry of the process very complicated. The typical pressures are in the range of 10 to 760 Torr and a carrier gas, most often hydrogen, is used to carry the precursors to the growth front.

MOVPE is cheaper than MBE and gives higher growth rates. However, most gases, especially, the group V precursors are very toxic.

Hydride vapor-phase epitaxy (HVPE) has become very popular for the fabrication of AlN, GaN, GaAs, InP semiconductors due to the high growth rate and the low cost of the synthesis [31]. As the name implies, the group V elements are transported using hydrides (AsH₃, PH₃, or NH₃) while the group III precursors are chlorides.

Aerotaxy is a relatively new method. Growth of nanowires occurs in a tube furnace without a substrate [32]. The advantage is very high growth rate, which is 100 – 1000 times faster than the substrate-based methods.

Combination of both approaches, or when *top-down meets bottom-up* is of particular interest. One of the examples is selective area epitaxy (SAE), which relies on the idea of bottom-up based nanowire growth on a patterned substrate which is fabricated using top-down approach [33]. For this, an amorphous mask layer (often SiN_x or SiO_x) is deposited on the substrate. Then holes, or the windows, are opened using lithography and etching. As a result, nanostructures grow selectively in these windows while no growth occurs on the mask since the deposited materials do not stick on the amorphous mask. This growth technique allows one to study the influence of individual growth parameters on nanowire growth, for instance the influence of pitch (the separation between the mask openings), which can modify the effective diffusion length of adatoms. This method is very important for growth of GaN nanowires for instance [34]. It is necessary to consider the growth (the growth rate) in terms of both group III and V elements through the probability for them to meet and incorporate into a growing monolayer [35]. The main challenge here is to find growth conditions that favour anisotropic nanowire growth instead of 2D layer growth (epitaxial lateral overgrowth).

An ordered array of nanowires can be fabricated using *nanosphere lithography* [36]. This method involves the formation of an array of spherical particles made of polystyrene or SiO₂ (bottom-up process), which pattern is transferred to the substrate (top-down process) [37]. Finally, one may use *block copolymers* [38] to fabricate vertical nanowires [39]. This method is based on the microphase separation of chemically different blocks. Depending on the composition of the block copolymer, spheres, cylinders, gyroids or lamellas might form [40]. Removing one of the polymers, cylindrical pores can be filled with material by electrodeposition, for instance [41].

1.2 Modelling strategies for nanowire growth

Theory did not fall behind the experiments. Understanding of the mechanism of nanowire growth has become the subject of considerable interest of many theorists.

This has led to the development of a number of analytical and numerical approaches for modelling the nanowire growth process. Unfortunately, the entire process involves so many steps that it is hard to describe it within a single model which would combine all of the elementary processes. These steps depend on a particular fabrication technique and may include homogeneous and/or heterogeneous reactions, heating and movement of precursors, elementary processes on the surface and in the liquid particle. Theoretical description is exacerbated by a set of parameters which influence on the elementary processes in a different way. For example, the diffusion flux is proportional to the droplet base perimeter, while the desorption is proportional to the droplet surface area, and both of them are temperature-dependent. Thus, existing models, utilizing various assumptions, are based on rate-limiting steps such as kinetics of the chemical reactions, thermodynamics and mass transport. As a result, different aspects of growth, for example the chemical composition, doping, growth rate or morphology, are often described independently. Finally, the initial governing equations are sometimes so difficult that an analytical solution is not possible and numerical calculations are required.

Theoretical studies can be divided into three big groups, namely one based on chemical equilibrium (I), nucleation models (II) and one, which considers growth as a kinetic process (III). They are schematically presented in Figure 1.3.

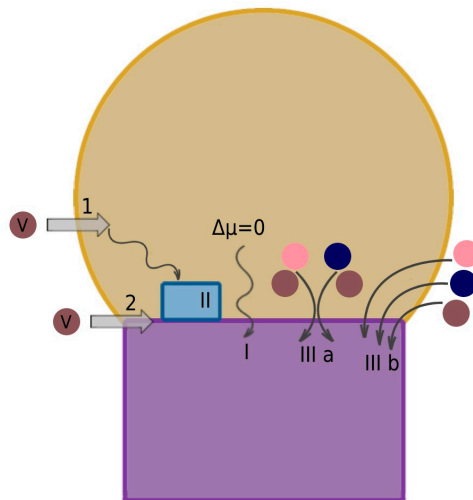


Figure 1.3. Scheme of nanowire growth within kinetic approach.

The central part of the first group of models is the thermodynamics of phase equilibrium, which provides the equilibrium chemical potential (and the equilibrium concentrations) at a fixed pressure and temperature.

Let us consider the classic example of growth of Au-catalyzed Si nanowires. The Au-Si phase diagram and a schematic growth procedure are presented in Figure 1.4. The first step is the formation of Au droplets (step I). The Au-Si liquid droplets can be formed as a result of feeding of the Au droplets by atoms of Si from the vapor phase after the pyrolysis of silicon tetrachloride ($SiCl_4 + 2H_2 \rightarrow Si + 4HCl$) [1]. If the influx of Si atoms exceeds its outflux, the concentration of Si atoms in the liquid particle increases and reaches the value c_L , which is higher than the equilibrium concentration (c_e) (step II). Then, the only way for the system to achieve the equilibrium state is by crystallization of Si which occurs at the liquid–solid interface under the droplet (step III). Continuing the process, the nanowire grows.

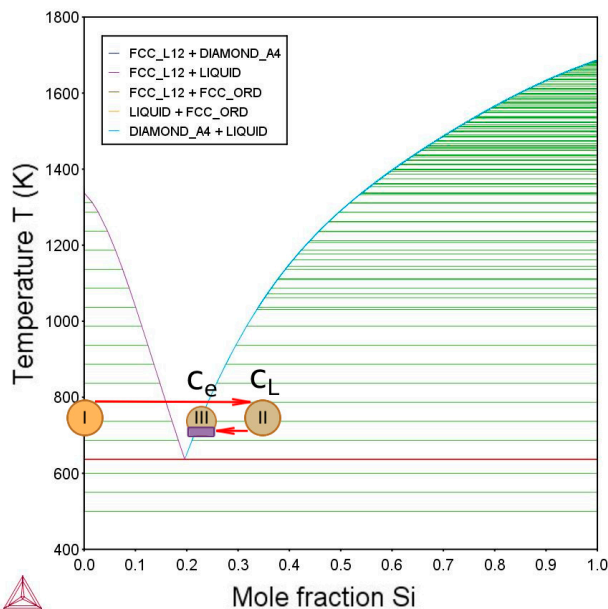


Figure 1.4. Au-Si phase diagram and growth of Au-catalyzed Si nanowires. The temperature doesn't change along the process (the arrows are drawn at different temperatures for clarity).

Assuming that the growth process occurs close to equilibrium $c_L \approx c_e$ (i.e. the situation when, once the equilibrium concentration has been achieved, all the arriving Si atoms incorporate into solid) one can find the relationship between the variables. So, the chemical composition of ternary III-V nanowires can be found by equating the chemical potentials of the liquid and solid phases (Section 3.3.1). One

may consider the equilibrium of the whole system (the chemical potential difference between the liquid and solid phases equals zero) or the equilibrium incorporation of each pair into the solid (the system of two equations). Clearly, the last one is a particular case of the first one.

The second group is based on the nucleus formation (Section 3.3.2). To describe growth, one should consider the formation energy of the nucleus, which consists of the chemical potential and surface energy terms [42].

The third group of models considers the growth process as a result of the dynamic incorporation of atoms or pairs of atoms (the so called two-component theory) into the solid. While within the first approach it was unimportant how atoms arrived to the droplet, the kinetic models consider various elementary processes such as the direct impingement, diffusion, evaporation and others. The point of this approach is to describe the incorporation rate of atoms or pairs. By doing this, one should introduce the most crucial elementary processes and estimate the number of arrived and departed atoms. Then, their difference will give the number of incorporated atoms.

Nanowire growth can be considered as nucleation followed by monolayer completion due to the incorporation of atoms into the growing monolayer [9] (mechanism III.a in Figure 1.3) or as a continuous process of elongation, where the nucleation stage is neglected (mechanism III.b in Figure 1.3) [43]. One of the disadvantages of the material balance models is a large number of unknown parameters ([43] for instance). For each experiment, these parameters need to be fitted. However, the majority of the models which describe the nanowire morphology is based on the material balance. Finally, there are the Monte-Carlo method [44] and other numerical methods [45] but they are out of the focus of this thesis.

Since the group V elements have very low solubility in the metal nanoparticle (its value is below the detection limit by energy-dispersive X-ray spectroscopy), the incorporation mechanism into the solid remains under lively debate. One possible pathway (and more commonly considered) is the incorporation through the catalyst droplet (mechanism 1 in Figure 1.3). In this case, the concentration of group V elements in the droplet is one of the governing parameters. Another mechanism involves two-dimensional interfacial diffusion along the solid-liquid interface between the droplet and the nanowire (mechanism 2 in Figure 1.3). Interestingly, a similar idea is used to describe the nanowire doping process [46]. In this thesis we consider the first pathway only.

1.3 Thesis outline

This doctoral thesis is devoted to the theoretical study of the chemical composition and crystal phase of ternary III-V nanowires with the main focus on vapor-liquid-solid growth. Starting from thermodynamic functions and phase transitions, then describing the vapor-liquid-solid mechanism, we will finish with the analysis of the liquid-solid composition dependence and the formation of a particular crystal phase. The effect of growth parameters including temperature, concentrations of Au and group V elements on the nanowire properties is studied in a systematic manner for several material systems relevant for nanowire growth. Theoretical approaches used for nanowire growth modelling include both kinetic and thermodynamic considerations.

The structure of this doctoral thesis is the following.

In **Chapter 2**, basic concepts in crystal growth are given including the fundamentals of nucleation theory and thermodynamics of phase transitions.

In **Chapter 3**, vapor-liquid-solid growth of nanowires is considered and different models used to describe the composition and crystal structure of ternary III-V nanowires are introduced.

In **Chapter 4**, the results of nanowire growth modelling are summarized and discussed.

In **Chapter 5**, concluding remarks and outlook on future research are presented.

At the end of the thesis, the published papers are appended.

2 Fundamentals of Nucleation Theory

The main purpose of this chapter is to give a brief introduction to classical nucleation theory, which serves as the foundation of the theoretical research and the developed models. First, thermodynamics of phase transition is described in Section 2.1. Section 2.2 is devoted to the Gibbs energy of substitutional solution phases. The formation energy of the nucleus is considered in Section 2.3. The chemical potentials in the solid and liquid in the case of multicomponent systems is described in Section 2.4. The miscibility gap is briefly introduced in Section 2.5. Finally, the surface energy is considered in Section 2.6.

2.1 Thermodynamics of phase transition

From the perspective of thermodynamics, the nanowire growth process occurs in an open system where the composition and amount of matter change. When optimal growth conditions are found and set up, temperature and pressure can be considered as constants. In such circumstances, it is convenient to describe changes in the state of a system in terms of the Gibbs free energy:

$$dG = VdP - SdT + \sum_{i=1} \mu_i dn_i. \quad (1)$$

Here G is the Gibbs free energy, T is temperature, S is entropy, V is volume, P is pressure, μ_i is the chemical potential of the species i and n_i is the number of species i .

Other thermodynamic quantities can be derived from the Gibbs free energy, including entropy, enthalpy, volume, heat capacity, thermal expansion, isothermal compressibility and, the most important, the chemical potential. The chemical potential of the component i is the partial derivative of the Gibbs free energy with respect to the amount of the i species, while pressure, temperature and all other species' concentrations in the mixture remain constant:

$$\mu_i = \left(\frac{\partial G}{\partial n_i} \right)_{P,T,n_{j \neq i}}. \quad (2)$$

The physical meaning of the chemical potential is the change of the Gibbs free energy of a homogeneous multicomponent system upon adding one mole of a certain component at constant pressure, temperature and system composition. Within the presented definition, the chemical potential is a partial molar property.

In relation to nanostructure growth, one of the most fundamental purposes of thermodynamics is to provide the relationship which would link the compositions of the various phases that are in contact with each other in an equilibrium system at constant temperature and pressure. A phase is a domain within which all relevant properties of a thermodynamic system such as chemical composition and density, are uniform. Two or more phases are in equilibrium if a set of conditions is fulfilled, namely there are equalities of temperatures (thermal equilibrium), pressures (mechanical equilibrium) and chemical potentials (chemical equilibrium). The Gibbs free energy of the system at equilibrium has a minimum value (alternatively, the entropy is maximized).

As an example, let us consider growth of InAs nanowires via the vapor-liquid-solid mechanism. Its phase diagram is shown in Figure 2.1a. The vapor-liquid condensation is possible when the difference of chemical potentials between the vapor and the bulk solid phase $\Delta\mu^{VS} = \mu_{InAs}^V - \mu_{InAs}^S$ is larger than the difference of chemical potentials between the liquid and the bulk solid phase $\Delta\mu^{LS} = \mu_{InAs}^L - \mu_{InAs}^S$. The liquid–solid crystallization is possible when the difference of chemical potentials between the liquid and the bulk solid phase is positive. Now let us fix the composition of the liquid droplet and calculate the chemical potentials. Figure 2.1b shows the chemical potentials in the case of the InAs materials system versus temperature at fixed As concentration of $c_{As} = 0.005$. Since we are interested in the liquid–solid crystallization, here and after we used the notation $\Delta\mu = \Delta\mu^{LS}$. As seen, the two curves cross at temperature $T_e = 426$ °C which is the equilibrium temperature at $c_{As} = 0.005$. The solid phase has the lower chemical potential in the temperature region below T_e whereas the liquid phase has a lower chemical potential at higher temperatures. Thus, the liquid–solid crystallization will occur only at temperatures $T < 426$ °C because in this case the system is out-of-equilibrium, so that it will strive towards its lowest energy state. As seen from Figure 2.1a, growth temperature can be increased using higher As concentrations. So, the equilibrium temperature is $T_e = 470$ °C at $c_{As} = 0.01$.

The driving force for the phase transition from a liquid state to a solid (which is at the equilibrium chemical potential) is determined by the chemical potential difference between the two phases $\Delta\mu = \mu^L - \mu^S$. In a dilute metastable system it can be expressed as $\Delta\mu = k_B T \ln(c/c_e) = k_B T \ln(\zeta + 1)$ with c being the concentration in the metastable phase and c_e being the corresponding equilibrium concentration. The term $\zeta = c/c_e - 1$ is called the supersaturation. For example, if the As concentration in the liquid $c_{As} = 0.015$, the supersaturation $\zeta = 2$ at $T = 426$ °C (since $c_{As,e} = 0.005$ at this temperature).

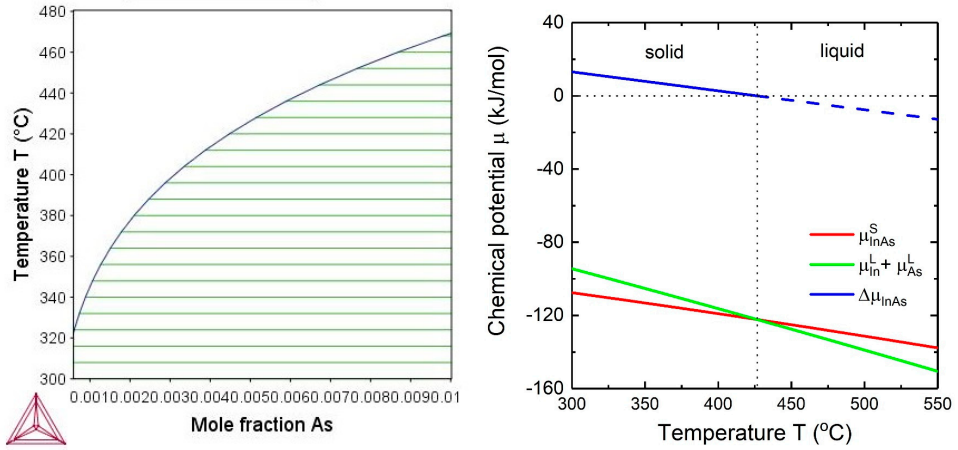


Figure 2.1. (a) In-As phase diagram. (b) Temperature dependence of the chemical potentials and the difference of the chemical potentials for InAs at $c_{As} = 0.005$.

2.2 Gibbs energy of substitutional solution phases

The Gibbs free energy of solution phases (solid or liquid) with N constituents is given by

$$G = \sum_{i=1}^N x_i G_i^0 + k_B T \sum_{i=1}^N x_i \ln x_i + G^E. \quad (3)$$

The first term is the sum of the Gibbs free energies of the pure elements G_i^0 with x_i the mole fraction of component i as weight. The second term describes the contribution of the configurational entropy within the assumption of the uniform distribution of species over the whole volume of the phase (the components are randomly mixed). These first two terms correspond to the case of an ideal solution, i.e. a solution in which the enthalpy of mixing is zero. Finally, the third term is the excess Gibbs energy G^E , which describes deviation from ideal solution behaviour when the enthalpy of mixing is non-zero.

Such deviation arises from different interactions between the mixture components, namely binary, ternary and high order interactions (see Figure 2.2). Thus, the excess Gibbs energy can be expressed as the sum of the binary excess Gibbs energy G_{bin}^E due to binary interactions, the ternary excess Gibbs energy G_{bin}^E due to ternary interactions and higher order excess energy G_{high}^E :

$$G^E = G_{bin}^E + G_{ter}^E + G_{high}^E. \quad (4)$$

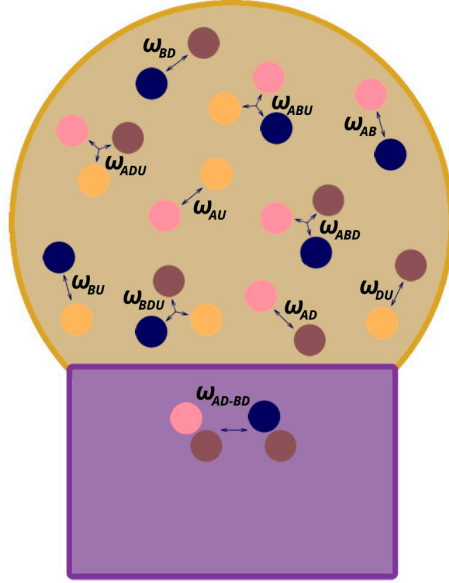


Figure 2.2. Schematic illustration of interactions in the liquid and solid.

The binary, ternary and high order excess Gibbs energies of a solution have the following form

$$G_{bin}^E = \sum_{i=1}^{N-1} \sum_{j=i+1}^N x_i x_j \omega_{ij}, \quad (5)$$

$$G_{ter}^E = \sum_{i=1}^{N-2} \sum_{j=i+1}^{N-1} \sum_{k=j+1}^N x_i x_j x_k \omega_{ijk}, \quad (6)$$

$$G_{high}^E = \sum_{i=1}^{N-3} \sum_{j=i+1}^{N-2} \sum_{k=j+1}^{N-1} \sum_{l=k+1}^N x_i x_j x_k x_l \omega_{ijkl} + \dots \quad (7)$$

Here x_i , x_j , x_k and x_l are the molar fraction of the constituent i , j , k and l respectively; ω_{ij} , ω_{ijk} and ω_{ijkl} are the binary, ternary and quaternary interaction parameters. Accounting for binary and ternary interactions is necessary for the correct description of multicomponent systems, whereas higher-order terms generally can be ignored in thermodynamic computations. Within the Redlich-Kister model, the interaction parameters can be expressed as:

$$\omega_{ij} = \sum_{m=0} (x_i - x_j)^m \omega_{i,j}^m, \quad (8)$$

$$\omega_{ijk} = v_i \omega_{i,j,k}^i + v_j \omega_{i,j,k}^j + v_k \omega_{i,j,k}^k \quad (9)$$

where

$$v_i = x_i + (1 - x_i - x_j - x_k)/3, \quad (10)$$

$$v_j = x_j + (1 - x_i - x_j - x_k)/3, \quad (11)$$

$$v_k = x_k + (1 - x_i - x_j - x_k)/3. \quad (12)$$

The form of the Eq. (9) ensures a symmetrical behaviour of the ternary interaction even in a multicomponent system. The index m in Eq. (8) denotes the order in the polynomial expansion.

The interaction parameters $\omega_{i,j}^v$ and $\omega_{i,j,k}^v$ are temperature-dependent. Usually, it is enough to present $\omega_{i,j}^v$ and $\omega_{i,j,k}^v$ as a linear temperature dependent parameters, i.e. $\omega_{i,j}^v = a_{ij}^v + b_{ij}^v T$ and $\omega_{i,j,k}^v = a_{ijk}^v + b_{ijk}^v T$ with the constants of a_{ij}^v , b_{ij}^v , a_{ijk}^v and b_{ijk}^v . Their values can be obtained from the parameter optimization in accordance with experimental data.

In the case of a ternary solid solution $A_xB_{1-x}D$, the enthalpy of mixing is described by the interaction parameter between AD and BD pairs in the solid, the so called the pseudobinary interaction parameter Ω . In a general case, it is composition-dependent and, according to Eq. (8), can be written down as

$$\Omega = \omega_s^0 + 2\omega_s^1(x - 0.5). \quad (13)$$

According to Stringfellow [47], the interaction parameter in the liquid can be found in terms of the electronegativities and solubility parameters of the pure components. Another method is a thermodynamic assessment within the CALPHAD method [48]. The methodology is as follows. First, all available experimental data for the chosen system should be collected and studied, including phase equilibria and thermochemical properties like enthalpy of mixing or formation energies. Next, the thermodynamic properties (the Gibbs free energies and interaction parameters) of each phase are described with a mathematical model (as discussed above). The unknown parameters are introduced in the form of $\omega_{i,j}^v = a_{ij}^v + b_{ij}^v T$ with a_{ij}^v and b_{ij}^v being adjustable constants. The adjustment of the model parameters is carried out by an optimization procedure so that the resulting parameter values together with the known parameters should reproduce the experimental data and the phase diagram.

As an example, consider the Au–P system. To the best of my knowledge, there are no published data on the Au–P interaction parameter in the liquid phase. However, this parameter is necessary for modelling the growth of Au-catalyzed $In_xGa_{1-x}P$ nanowires, which are very promising for the fabrication of photovoltaic devices, such as tandem solar cells. The values of the Gibbs free energies of the pure

substances, Au and P, can be found in [49] while the Au-P phase diagram is presented in [50].

For the thermodynamic assessment, specific software products are utilized. There are several commercial products including MTDATA [51], Thermo-Calc [52], FactSage [53], and Pandat [54]. There is also an open source software, OpenCalphad [55]. In our case the optimization was performed in the PARROT module of the Thermo-Calc software. The optimized interaction parameter is given by $\omega_{AuP} = 7651.5$ J/mol. As can be seen from Figure 2.3, one parameter only is enough for correct reproduction of the phase diagram.

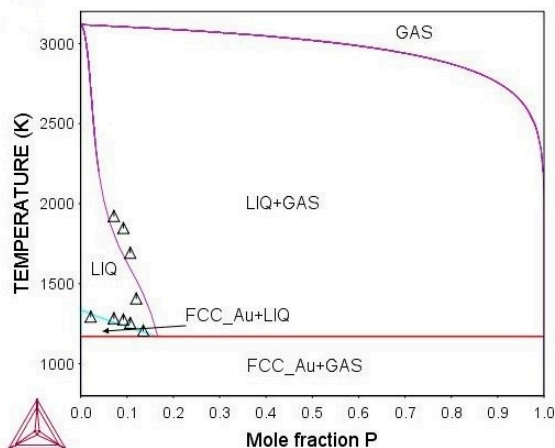


Figure 2.3. Calculated Au-P phase diagram. The triangles represent experimental data taken from [50].

2.3 Formation energy

It is widely established that nanowire growth occurs as a result of a nucleus forming and its subsequent growth into a 2D layer [9]. Here and after, 2D means that the layer is of monomolecular layer height. Normally, the growth time (the time needed to complete a monolayer) is shorter than the time between two nucleation events. As a result, a nanowire grows in the layer-by-layer regime. However, the preferential nucleation site could be at the triple line (the edge of the growth interface, where all the three phases meet) or in the center of the growth interface [56], depends on the growth conditions.

In the general case, the change of Gibbs energy associated with the nucleus formation is given by

$$F = -\Delta\mu s + \Gamma P_N h + \gamma_{LV}\Delta S. \quad (14)$$

Here $\Delta\mu$ is the chemical potential difference between the liquid particle and the solid nucleus and s is the number of III-V pairs in the nucleus, Γ is the effective surface energy, P_N is nucleus perimeter and h is layer height. The first term describes the energy released by increasing the volume of the nucleus. The second term corresponds to the surface free energy due to creation of an interface between the new phase and the metastable initial phase. The last term is a VLS specific term and refers to the change of the drop surface ΔS due to the island formation where γ_{LV} is the liquid-vapor surface energy.

Ignoring the third term, Eq. (14) can be re-written as

$$F = -\Delta\mu s + a\sqrt{s}. \quad (15)$$

Clearly, the energy released due to the liquid-solid transition is proportional to the nucleus size ($\sim s$), while the cost of forming new surfaces is proportional to the nucleus perimeter ($\sim\sqrt{s}$). This means the first term grows faster than the second one. Since they have opposite signs, the formation energy has a maximum. The nucleus tends to decay at the left side of this maximum (the subcritical region) and to grow at the right side of this maximum (the supercritical region). At the maximum, the probabilities of the both processes are equal. The formation energy which corresponds to this maximum is called the nucleation barrier, while the corresponding size is called the critical size. Figure 2.4 shows the formation energy of an InAs nucleus as a function of its size calculated at different As concentrations and at $a \approx 2.54$ eV. As seen, the critical size decreases with an increase of As concentration (the contribution of the first term is higher).

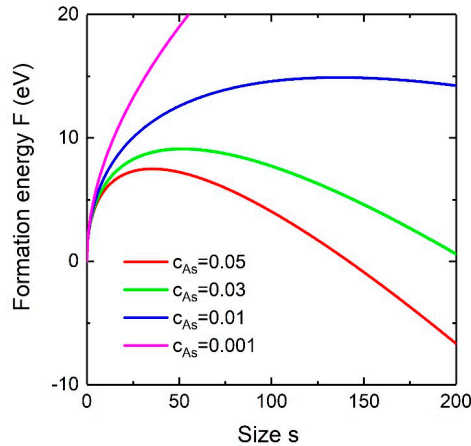


Figure 2.4. Formation energy of InAs nucleus at $T = 350$ °C and at different As concentrations.

2.4 Chemical potentials in multicomponent systems

With the exception of the approach based on the materials balance, all the models for ternary nanowire formation include the chemical potentials. To describe the most general case, we should consider the formation of ternary $A_xB_{1-x}D$ nanowires from a quaternary liquid droplet which consists of A, B, D, and U, where U is a solvent. As it follows from the notation, x denotes the AD concentration in the solid, and is called the solid composition. Correspondingly, $(1 - x)$ denotes the BD concentration in the solid. To be incorporated into the solid, the liquid must be supersaturated with respect to the solid. The differences of chemical potential which correspond to the AD and BD pairs ($\Delta\mu_{AD}$ and $\Delta\mu_{BD}$, respectively) can be written down as

$$\Delta\mu_{AD} = \mu_A^L + \mu_D^L - \mu_{AD}^S, \quad (16)$$

$$\Delta\mu_{BD} = \mu_B^L + \mu_D^L - \mu_{BD}^S. \quad (17)$$

Here, L and S , denote the liquid and solid phases, respectively; μ_A^L , μ_B^L and μ_D^L are the chemical potentials of atom A, B and D in the liquid, respectively; μ_{AD}^S and μ_{BD}^S are the chemical potentials of the AD and BD pairs in the solid, respectively.

According to the definition of the chemical potential, the chemical potentials of the atoms in the liquid can be found by differentiating the Gibbs free energy of the liquid solution G^L . Expressing in terms of concentrations, the chemical potentials of the constituent i can be presented in the form

$$\mu_A^L = G^L + \frac{\partial G^L}{\partial c_A} - \sum_{i=1}^N c_i \frac{\partial G^L}{\partial c_i}, \quad (18)$$

$$\mu_B^L = G^L + \frac{\partial G^L}{\partial c_B} - \sum_{i=1}^N c_i \frac{\partial G^L}{\partial c_i}, \quad (19)$$

$$\mu_D^L = G^L + \frac{\partial G^L}{\partial c_D} - \sum_{i=1}^N c_i \frac{\partial G^L}{\partial c_i}. \quad (20)$$

where, according to Eq. (3), the Gibbs free energy of the liquid solution is given by

$$\begin{aligned} G^L = & \sum_{i=1}^N c_i \mu_i^0 + RT \sum_{i=1}^N c_i \ln c_i + \sum_{i=1}^{N-1} \sum_{j=i+1}^N c_i c_j [\omega_{i,j} + \omega'_{i,j}(c_i - c_j)] \\ & + \sum_{i=1}^{N-2} \sum_{j=i+1}^{N-1} \sum_{k=j+1}^N c_i c_j c_k \omega_{ijk}. \end{aligned} \quad (21)$$

Here c_i is the concentration (atomic fraction) of element i in the liquid phase, μ_i^0 is the chemical potential of pure component i in the liquid; $\omega_{i,j}$ is the composition-independent (or, zero-order) interaction parameter $\omega_{i,j}^0$ (thus, $\omega_{i,j} = \omega_{j,i}$) and $\omega'_{i,j}$ is the first-order interaction parameter (thus, $\omega'_{i,j} = -\omega'_{j,i}$).

The chemical potentials of the AD and BD pairs in the solid can be presented in the form

$$\mu_{AD}^S = \mu_{AD}^0 + RT \ln x + (1-x)^2[\omega_S + (4x-1)\omega'_S], \quad (22)$$

$$\mu_{BD}^S = \mu_{BD}^0 + RT \ln(1-x) + x^2[\omega_S + (4x-3)\omega'_S]. \quad (23)$$

Here μ_{AD}^0 and μ_{BD}^0 are the chemical potentials of pure AD and BD binaries, respectively. Comparing with Eq. (13), here we used the notations $\omega_S = \omega_S^0$ and $\omega'_S = \omega_S^1$.

Finally, the chemical potential difference between the mother (liquid) and daughter (solid) phases can be written as

$$\Delta\mu = x\Delta\mu_{AD} + (1-x)\Delta\mu_{BD}. \quad (24)$$

2.5 Miscibility gap

In the classical nucleation theory for a ternary material, two characteristic curves, namely the binodal and spinodal, play an important role. The binodal separates the single-phase state region from a region where two distinct phases may coexist. The binodal which separates the homogeneous solid solution from the miscibility gap region is called solvus. In the case of a ternary alloy, to find it, one should calculate the derivative of the Gibbs free energy of with respect to solid composition x and equate the result to zero. So, within the regular solution model, ignoring possible composition-dependent parameters (ω'_S , for instance), the binodal (solidus in this case) can be written in the form

$$T_b = \frac{\omega_S(1-2x)}{R \ln \frac{1-x}{x}} \quad (25)$$

with R being the gas constant.

The second curve, the spinodal, represents the limit of absolute instability between phases. It is defined by the condition that the second derivative of the Gibbs free energy is zero and takes the form

$$T_{sp} = 2 \frac{\omega_S}{R} x(1-x). \quad (26)$$

It can be noticed that the spinodal is always under the binodal except of the critical point where they meet. This critical point is in the center (i.e $x = 0.5$) if $\omega'_S = 0$.

An example of the binodal and spinodal lines for $\text{In}_x\text{Ga}_{1-x}\text{As}$ alloy calculated using Eq. (25) and (26) is presented in Figure 2.5.

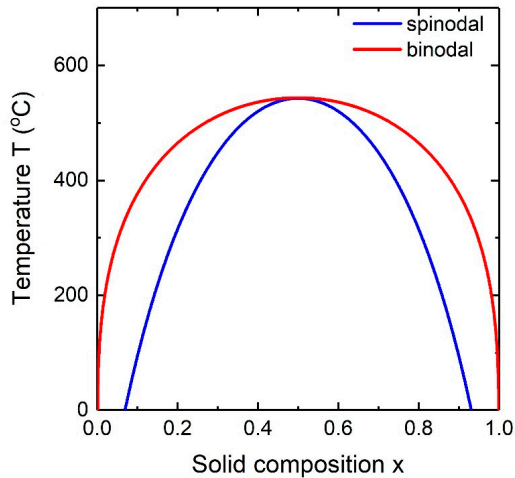


Figure 2.5. The binodal and spinodal lines calculated for $\text{In}_x\text{Ga}_{1-x}\text{As}$ alloy.

The composition above the binodal corresponds to a stable homogeneous solid solution. The region between the binodal and spinodal lines corresponds to a metastable state: the homogeneous solid solution can persist at small enough fluctuations. Finally, under the spinodal line, arbitrarily small fluctuations in the system lead to phase separation via the so called spinodal decomposition mechanism.

According to Eq. (25), the pseudo-binary interaction parameter is a key parameter which defines the width of the miscibility gap region: the larger its value, the bigger the miscibility gap and the higher the critical temperature, above which the miscibility gap vanishes. Accounting for the second Redlich–Kister polynomial parameter ω'_S and higher, i.e. introducing composition-dependent terms, leads to an asymmetrical shape of the miscibility gap.

2.6 Surface energy

Nucleation involves the formation of new interfaces which divide the nucleus from other phases. The number of the interfaces depends on the shape of the nucleus; and for simplicity, let's consider a triangular nucleus of thickness h . There are two qualitatively different areas for nucleation, namely nucleation at the edge of the solid-liquid interface (at triple phase line, or TPL) and nucleation in the center of the solid-liquid interface (C). The configuration is schematically presented in Figure 2.6.

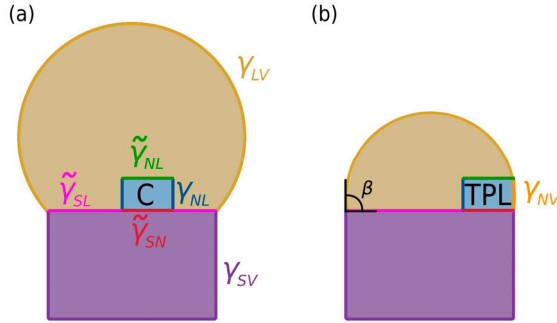


Figure 2.6. Nucleation of island in position in the center of the liquid-solid interface (a) and at the triple phase line (b).

The contribution of the surface energy of the nucleus into the formation energy is given by

$$F^{surf} = A(\tilde{\gamma}_{NL} - \tilde{\gamma}_{SL} + \tilde{\gamma}_{SN}) + \Gamma P_N h. \quad (27)$$

For subscripts the following notation is used: N denotes the nucleus, L – liquid, S – solid and V – vapor. The first term describes a change of free energy due to the bottom and top surface with area A . Since the atomic configuration of the nanowire-liquid and nucleus-liquid interfaces are the same leading to $\tilde{\gamma}_{NL} = \tilde{\gamma}_{SL}$, the first two terms in the brackets vanish. The second term describes the contribution of the lateral surface of the nucleus having a perimeter P_N . In the general case, the surface energy Γ related to the nucleus sidewalls is given by

$$\Gamma = \chi\gamma_{NL} + (1 - \chi)(\gamma_{NV} - w\gamma_{LV}). \quad (28)$$

Here χ is the fraction of the edge length of the nucleus which is not in contact with the vapor phase. From the geometrical considerations, $w = \Omega_L/\Omega_S \sin \beta$ with β being the contact angle, Ω_L and Ω_S being the volume per III–V pair in the liquid and solid. Later on wurtzite (WZ) and zinc-blende (ZB) crystal phases will be introduced. Since the nucleus-vapor surface energy γ_{NV} for the wurtzite and zinc-

blende phases differ [57], [58] it can be presented as $\gamma_{NV} = \gamma_{SV}\tau_P$ with $\tau_{ZB} = 1$ and $\tau_{WZ} < 1$. Summarising, the effective surface energy of the nucleus can be re-written as

$$\Gamma = \chi\gamma_{SL} + (1 - \chi) \left(\gamma_{SV}\tau_P - \gamma_{LV} \frac{\Omega_L}{\Omega_S} \sin \beta \right). \quad (29)$$

Here γ_{SL} , γ_{SV} and γ_{LV} are the surface energies of the solid-liquid, solid-vapor, and liquid-vapor interfaces, respectively. Eq. (29) describes both nucleation in the center and at the triple phase line. Indeed, if the nucleus lateral surface is entirely surrounded by the liquid then $\chi = 1$ and $\Gamma^C = \gamma_{SL}$. On the other hand, if the nucleus is triangular and one lateral surface of the nucleus is in contact with the vapor, then $\chi = 2/3$ and $\Gamma^{TPL} = 2/3\gamma_{SL} + 1/3(\gamma_{SV}\tau_P - \gamma_{LV}\Omega_L/\Omega_S \sin \beta)$.

For further analysis, a number of parameters could be estimated using Vegard's law. So, the liquid-vapor surface energy writes down as

$$\gamma_{LV} = c_A\gamma_{LV}^A + c_B\gamma_{LV}^B + c_D\gamma_{LV}^D + c_U\gamma_{LV}^U. \quad (30)$$

Using the previously introduced notation ($y = c_A/c_{tot}$), this can be re-written as

$$\gamma_{LV} = yc_{tot}\gamma_{LV}^A + (1 - y)c_{tot}\gamma_{LV}^B + c_D\gamma_{LV}^D + (1 - c_{tot} - c_D)\gamma_{LV}^U. \quad (31)$$

Contribution of group V elements can be ignored due to a small value of its concentration.

Next, the volume per III–V pair in the solid is given by

$$\Omega_S = x\Omega_S^{AD} + (1 - x)\Omega_S^{BD}. \quad (32)$$

Here $\Omega_S^{AD} = a_{AD}^3/4$ and $\Omega_S^{BD} = a_{BD}^3/4$ are the volume per AD and BD pairs in the solid with a_{AD} and a_{BD} being the lattice constants of AD and BD, respectively. It is worth noting that $\Omega_S = (N_{AD}\Omega_S^{AD} + N_{BD}\Omega_S^{BD})/s$ where N_{AD} and N_{BD} are the number of AD and BD pairs in the solid. Vegard's law is used to estimate the volume per III–V pair in the liquid.

Finally, the perimeter of the equilaterally triangular nucleus is $P_N = 3r$, where the side length r can be presented as

$$r = \frac{2}{3^{1/4}\sqrt{h}} \sqrt{N_{AD}\Omega_S^{AD} + N_{BD}\Omega_S^{BD}}. \quad (33)$$

Returning to Eq. (14) and (15), the following substitution has been used

$$a = 2 \cdot 3^{3/4} \Gamma \sqrt{\Omega_S h}. \quad (34)$$

3 Vapor-Liquid-Solid Growth of Nanowires

The main purpose of this chapter is to introduce ternary nanowires, their controllable properties, including the chemical composition and crystal structure, and several models used to describe them. Section 3.1 is devoted to the vapor–liquid–solid mechanism, its stages and elementary processes during nanowire growth. A special attention is paid to the tuneable properties of nanowires. A brief description of the recent progress and several control-related issues are given. Ternary nanowires are introduced in Section 3.2. Next, the models predicting the chemical composition of ternary nanowires are presented in Section 3.3. They are the equilibrium model (Section 3.3.1), nucleation model (Section 3.3.2), incorporation model (Section 3.3.3) and material balance model (Section 3.3.4). Finally, Section 3.4 starts the discussion on the crystal phase of III-V nanowires.

3.1 Vapor–liquid–solid mechanism

Among the broad spectrum of growth methods offered by bottom-up and top-down approaches, briefly considered in Section 1.1, vapor-liquid-solid growth remains the most popular for the fabrication of nanowires. This growth mechanism combines the advantages of the bottom-up approach and self-assembly with benefits from the usage of the liquid phase as an intermediate one. This gives more freedom to tailor physical and chemical properties of nanostructures making vapor-liquid-solid growth versatile and flexible. Briefly, one might tune the nanowire morphology (both the radius and length), chemical composition, doping, heterostructure interface, crystal phase, density and position on the substrate.

The nanowire size can be accurately controlled [59], which is especially important if one is interested in their size-dependent properties. Due to the layer-by-layer regime, the radius can be effectively controlled along the nanowire through tuning the size of the liquid particle. Thus, the nanowire shape can be changed under self-catalyzed growth, while in the case of Au-catalyzed nanowires, the radius remains constant being mainly determined by the initial size of the catalyst droplet. However, dealing with an array of nanostructures, one should consider the radius

distribution, which is often non-uniform due to the initial size distribution of the droplets [60]. In its turn, it may cause the broadening of the length distribution because the elongation rate often depends on the radius. For example, in the case of diffusion-induced growth of Au-catalyzed nanowires the length is inversely proportional to the radius, which means that thicker nanowires grow slower than thinner ones [61]. This is because the diffusion flux is proportional to perimeter of the nanowire tip ($\sim R_{NW}$) while the elongation rate is proportional to the area of the nanowire tip ($\sim R_{NW}^2$). Another source of the broadening of the length distribution is a delay in the nanowire nucleation stage [62], which results in a long tail of the distribution [63]. Self-catalyzed growth is very attractive due to the self-focusing effect [20], [21], [60]. It involves narrowing of the nanowire radius up to a certain stationary radius regardless of the initial size of the droplet. The self-focusing effect allows one to improve the size uniformity of a nanowire ensemble. Overall, Poissonian and sub-Poissonian size distributions might be achieved [64]. However, there are issues related to vapor-solid growth on sidewalls and uncontrollable tapering [65].

Another property of nanowires which can be tuned is the chemical composition [66], [67]. Obviously, this concerns ternary and quaternary nanowires. The chemical composition is probably the most crucial parameter because it determines the bandgap [68]. So, any bandgap between those of the binary compounds can be obtained by tuning the alloy composition according to the requirements of specific applications [69]. Moreover, while the bandgap engineering in planar epitaxial structures is limited by the lattice mismatch [70], [71], [72], the effective relaxation due to small nanowire footprints solves this issue making possible to combine highly mismatched materials without the formation of defects [73]. However, to grow some of the III-V nanowires one should use stems consisting of other materials [74]. In theory, one can control the solid composition by varying the vapor composition. This topic is of current interest because the vapor-solid composition dependence is rarely trivial. With the exception of some cases [75] when the solid composition is almost proportional to the vapor one, the composition dependences are often very steep and non-linear. The reason is a large number of elementary processes which depend on different parameters such as temperature, droplet shape and size, flux ratio, pitch and others. Another problem is miscibility [76] when the binary compounds tend to segregate forming domains of pure compounds. This is a common problem for bulk structures while, it seems, the miscibility gap in nanowires can be suppressed under high supersaturation conditions (*Paper IV*), [77].

Varying the composition of the vapor phase during vapor-liquid-solid growth, one can obtain axial heterostructures in nanowires [78]. Its key feature is the interface abruptness, which should be as sharp as possible for many applications. However, even if one could switch the gas fluxes instantly, the material remains in the liquid droplet and continues to incorporate into the solid preventing the formation of sharp

interfaces. This reservoir effect [79] explains experimentally observed smooth heterointerfaces in $\text{III}_x\text{III}_{1-x}\text{V}$ nanowires [80], [81]. Since the total concentration of group V elements in the liquid is very small, it is possible to form almost atomically sharp heterointerfaces in $\text{IIIV}_x\text{V}_{1-x}$ nanowires, for instance in InP-InAs heterostructured nanowires [82].

The formation of *pn*-junctions in nanowires is possible due to controllable doping of nanowires. There are several difficulties such as non-ideal abruptness and the inhomogeneity of the dopant distribution. So, using electron holography it has been shown that the dopant atoms can incorporate inhomogeneously over the nanowire radius and the length. For example, Be incorporates into the {112A} sidewall facets leading to the three-fold symmetric dopant distribution [83]. The inhomogeneity over the nanowire length might be explained by a combination of the following factors: (i) simultaneous vapor-solid radial and vapor-liquid-solid axial growth, (ii) dopant atoms are mainly incorporated by the vapor-liquid-solid process [84]. The possibility to dope various materials and synthesize heterostructured nanowires gives an unlimited number of possible combinations.

One of the most unique features of nanowires is control of the crystal structure [85], [86], [87]: while in bulk, the majority of III–V semiconductors such as GaAs, InP and GaP exhibits a cubic zinc blende structure, nanowires can form a hexagonal wurtzite structure. With the development of growth techniques, nanowires with a single crystal structure or modulated one can be obtained. Modern *in-situ* measurement methods allow us to get a look into the growth process [8], [9], [10]. Recently, an astonishing progress has been made in crystal phase engineering: structures with atomically controllable crystal phase superlattices have been grown and presented by Dick [88]. It has been shown that crystal phase engineering (controllable switching between different crystal structures) can be achieved by varying the growth conditions: the flux ratio and temperature [86], [87].

Finally, one may control the nanowire density and position on the substrate. So, it is possible to change the nanowire density by tuning the substrate temperature during the formation of the liquid particles [42]. A high degree of control has been achieved using a patterned amorphous layer [89]. Both the density (and, thus, the distance between nanowires) [90] and position of nanowires (because of the materials competition [91] and shadow effect [92]) have effect on the diffusion flux from the substrate: nanowires compete for the adatoms on the substrate if the distance between nanowires is smaller than the diffusion length.

The basic idea of vapor-liquid-solid growth is that growth at the liquid-solid interface is much faster than growth on the non-activated substrate surface. The main principles have not been changed since the first experiments of Wagner and Ellis in 1964 [1]. The first step involves preparation of the substrate. It might include the evaporation of the oxide protective layer and growth of the buffer layer to get rid of the substrate defects (Figure 3.1a). One might also pattern an amorphous (e.g.

oxide) layer with an array of holes (right half of Figure 3.1a). Nanowire growth is possible in the holes only. The second one is the formation of an array of the liquid droplets (Figure 3.1b) [93]. Due to its versatility, gold remains one of the most popular catalysts. By doing this, a thin film of Au is deposited on the substrate. Heating the substrate above a certain temperature (which can be lower than the Au melting temperature due to the nanoparticle interaction with the substrate forming a eutectic), the Au film melts forming the droplets. This is one of the requirements of the catalyst. Next step is the deposition of semiconductor materials which feed the droplets. Under supersaturation conditions, crystallization occurs at the liquid-solid interface leading to the formation of nanowires (Figure 3.1c). In total, there are two crossings of phase boundaries, namely the vapor-liquid and liquid-solid ones, which explains the name of the growth mechanism.

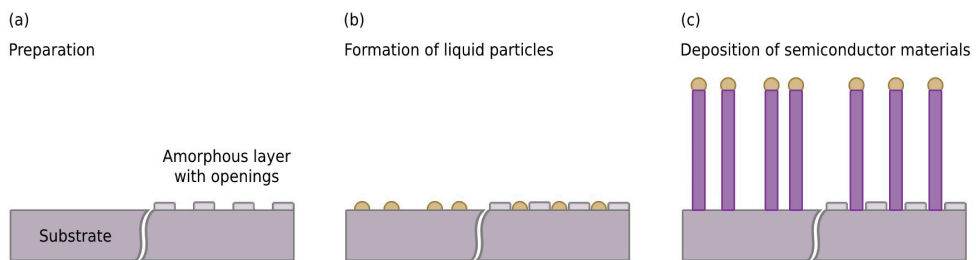


Figure 3.1. Schematic illustration of different stages of the vapor-liquid-solid growth mechanism on the example of Au-catalyzed nanowires.

There are many elementary processes which occur during vapor-liquid-solid growth (see Figure 3.2). Some of them feed the droplet, namely the direct atomic flux (1), the diffusion flux from the substrate (2) and from the nanowire sidewalls (3), re-emission (4), i.e. the flux of atoms to the droplet evaporated from the substrate and the sidewalls of other nanowires. The sink of the atoms from the droplet is determined by the nanowire elongation rate (5) (as a result of nucleation and monolayer completion), the desorption from the droplet (6) and the reverse diffusion (7). There might be growth on the sidewalls (8), the evaporation from the sidewalls (9), parasitic growth on the substrate (10) and diffusion from the substrate to the sidewalls (11).

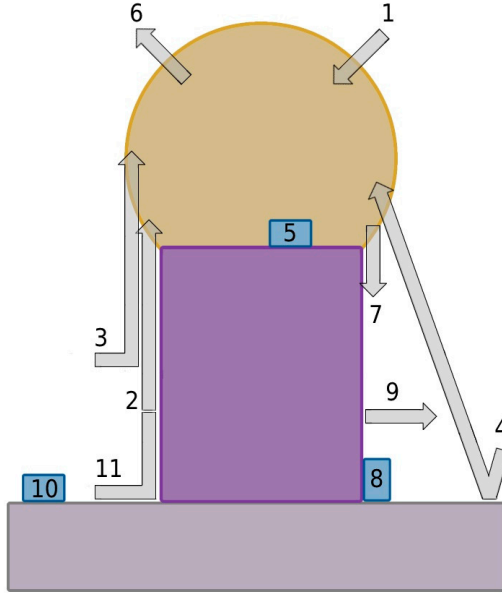


Figure 3.2 Schematic illustration of elementary processes occurring during vapor-liquid-solid growth of nanowires.

3.2 Ternary nanowires

Ternary III-V alloys formed between binary compounds represent an important category of semiconductors. The ability to grow ternary solid solutions (structures composed of two binary semiconductors which have the same cation or anion) has opened new horizons [94], [95], [96]. Discrete bandgap values of elemental and binary compound semiconductors have been replaced by the possibility to choose the required one from a continuous range of values [68]. This is possible due to the change of proportion between two binary semiconductors in a solution, or simply put, varying the solid composition. The solid composition primarily depends on the vapor phase composition and growth temperature.

The lattice parameter of a ternary solid solution $A_xB_{1-x}D$ is approximately a weighted mean of the two constituents lattice parameters at the same temperature:

$$a_{A_xB_{1-x}D} = xa_{AD} + (1 - x)a_{BD}. \quad (35)$$

Here, a_{AD} and a_{BD} are the lattice parameters of the AD and the BD binary semiconductors respectively. This linear relationship is known as Vegard's law [97].

In many ternary semiconductor systems, the band gap is approximately also a linear function of the lattice parameter. Thus as a first approximation, the band gap of the

ternary solid solution $E_{A_xB_{1-x}D}^g$ can be calculated by means of Vegard's law. However, the band gap of the majority of ternary systems is well modelled by the quadratic equation

$$E_{A_xB_{1-x}D}^g = xE_{AD}^g + (1-x)E_{BD}^g - \tilde{b}x(1-x). \quad (36)$$

Here, E_{AD}^g and E_{BD}^g are the band gaps of the AD and the BD binary semiconductors respectively and \tilde{b} is the bowing parameter.

Besides of bandgap tuning, a number of properties of the final structure changes with the composition, such as the lattice parameter, the density of states and the optical properties.

However, not all solid compositions are thermodynamically stable during growth. At some concentrations, the growth of domains composed of pure binary compounds is more energetically favourable. Thus, at such conditions, the formation of a homogeneous ternary solid solution is thermodynamically forbidden. In spite of the fact that in the macroscopic point of view the average composition will be as it is required, the real optical and electronic properties will significantly differ being some combination of binary compounds. It reduces the structural quality and the efficiency of the final nanowire-based device. This range of the forbidden compositions is called the miscibility gap and is observed in structures of different dimensions including bulk structures, thin films and nanowires. By growing the material far from thermodynamic equilibrium, even compositions within the miscibility gap can be reached.

3.3 Nanowire composition

In multicomponent nanowires, the bandgap is the most crucial parameter for the majority of applications including photodetectors, lasers, sensors and solar cells. As mentioned above, the bandgap is determined by the solid composition. Thus, understanding the key underlying principles of the formation of ternary nanowires and its quantitative description are a milestone for the successful development of optoelectronic device technology associated with nanowires.

Due to the great interest in this topic, a large number of different approaches for modelling of the chemical composition of nanowires has been developed. However, there is no well-established classification system nor approved names for some of the models, but here I make an attempt to classify them in four groups. The first group, which includes the equilibrium (section 3.3.1) and nucleation (section 3.3.2) models deals with pure thermodynamics: growth occurs as a result of a quasi-static process during which the system remains close to equilibrium. In such a case the thermodynamic functions are used to describe the process and to determine the

thermodynamic properties. The kinetic approach is very opposite to the thermodynamic one. It considers a non-equilibrium state and relies on the idea that the solid composition is determined by the time-dependent incorporation rates of AD and BD pairs (Section 3.3.3) or A, B and D components (Section 3.3.4). Very often the models are coupled to the materials balance in the system. Finally, one may employ Monte Carlo approach [44].

The presence of the large number of models might be explained by the complex character of nanowire growth. So, there is plenty of room for different kinds of simplifications and assumptions while depending on the conditions there are different limiting steps. For example, the growth rate can be limited by thermodynamics at high temperatures while the chemical reaction rates can limit nanowire growth at low temperatures. There might be the case of the mass transport limitation at temperatures in between. These limiting steps are attributed to and well understood for thin films [98], but they should be relevant for nanowires too [99], [100]. An interesting case limited by the kinetics of atoms is growth of InAs nanowires in SiO₂ nanotube templates [101].

Each model has its advantages and disadvantages. For example, there are no fitting parameters in the equilibrium model, which means that no estimation of the unknown parameters is needed. Thus, in theory, the model should predict experimental observations reliably. On the other hand, such a model can be an oversimplification of the growth process. It is widely known that the results can vary from growth machine to growth machine. Then, for quantitative results one should not use such models because of their inflexibility. On the other side, the results from the models which include too many fitting parameters might be meaningless in terms of overfitting of the experimental data.

Despite the different approaches, the modelling system remains the same. The nucleation and completion of a monolayer resulting in growth of a ternary (AD)_x(BD)_{1-x}=A_xB_{1-x}D nanowire occur from a multicomponent liquid particle situated on the nanowire tip. Growth is schematically presented in Figure 3.3. The droplet might be either quaternary consisting of A, B, D and U components or ternary consisting of A, B and D components. According to the definition, the solid composition x is defined by the AD content in the solid, namely $x = N_{AD}/(N_{AD} + N_{BD})$ with N_{AD} and N_{BD} being the numbers of AD and BD pairs in the solid, respectively. For simplicity, the ratio $y = c_A/(c_A + c_B)$ is called the liquid composition.

Formally, we consider the vapor-liquid-solid growth mechanism. However, with the exception of the model based on the material balance, we are interested in the liquid-solid phase transition and ignore the vapor-liquid one. Moreover, we start our analysis considering a nanowire with a non-zero length. In other words, we ignore the initial stage of nanowire nucleation.

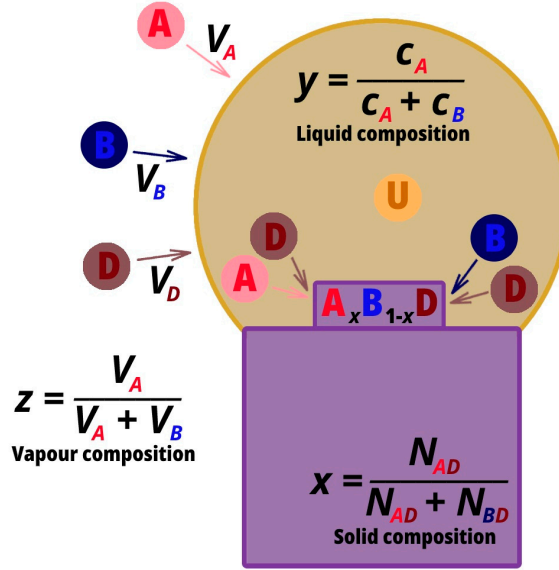


Figure 3.3. Schematic illustration of the growth process of a ternary $A_xB_{1-x}D$ nanowire from a quaternary liquid melt.

3.3.1 Equilibrium model

The core idea of the first approach is that the incorporation of AD and BD pairs into the solid is considered separately, but both processes occur at equilibrium:

$$\Delta\mu_{AD} = 0, \quad (37)$$

$$\Delta\mu_{BD} = 0. \quad (38)$$

In the case of self-catalyzed growth at fixed temperature, the thermodynamic system is fully described by three variables, namely the solid composition, and the concentration of D and A components (because $c_B = 1 - c_A - c_D$). The last one can be replaced by the liquid composition y . At equilibrium, there is only one arbitrary variable. In the case of Au-catalyzed growth, one needs to consider the Au concentration as a parameter. Figure 3.4 shows the dependence of the solid composition on the liquid composition (a) and the As concentration (b) for self-catalyzed $In_xGa_{1-x}As$ nanowires for different temperatures. For simplicity, solving Eqs. (37) and (38) we ignore the ternary and composition-dependent binary interaction parameters. As seen, to vary the solid composition in a wide range, high concentration of indium in comparison with gallium is needed. Low concentration of As in the droplet is the well-known result in the case of nanowire growth via the vapor-liquid-solid mechanism. Usually, its concentration is so low that it is impossible to detect it during growth. Increasing temperature, the InAs content in the solid increases at fixed indium concentration in the droplet. It is the opposite for

As concentration: the InAs content decreases with the temperature. This approach has been extensively used for the description of nanowire growth [94].

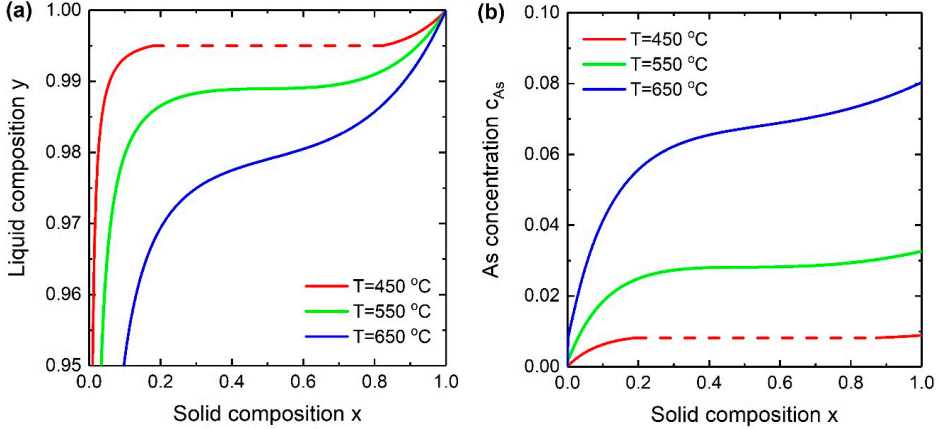


Figure 3.4. The solid composition versus the liquid composition (a) and the As concentration (b) for self-catalyzed $\text{In}_x\text{Ga}_{1-x}\text{As}$ nanowires for different temperatures. The dashed curve corresponds to the miscibility gap.

3.3.2 Nucleation model

The nucleation model relies on the idea that nanowire growth occurs as a result of the formation of a small nucleus, which rapidly spreads out laterally over the entire liquid-solid interface [9]. The key object is the critical nucleus being a two-dimensional solid particle which has the equal probability to grow or decay. Adding one more monomer to the critical nucleus, it becomes stable. It is in unstable equilibrium with a supersaturated environment constituted by the liquid droplet. To apply the model for the nanowire composition, one should assume that the monolayer composition coincides with the composition of the critical nucleus.

Within the model, the nucleation rate is assumed to be entirely controlled by the height of the nucleation barrier. The critical nucleus is defined by the solid composition and the size, i.e. the number of AD and BD pairs in the solid. To find them, one should simultaneously maximize the formation energy in the size and minimize it in the solid composition. Then, the system of the partial differential equations writes down as

$$\frac{\partial F}{\partial x} = 0, \quad (39)$$

$$\frac{\partial F}{\partial s} = 0. \quad (40)$$

Substituting the formation energy (Eq. (15)), the system of the equations can be rewritten in the form

$$-\frac{\partial\Delta\mu}{\partial x}s + \frac{da}{dx}\sqrt{s} = 0, \quad (41)$$

$$-\Delta\mu + \frac{a}{2\sqrt{s}} = 0. \quad (42)$$

Here a is the effective surface energy of the ternary nucleus (for details, see *Paper V*). Maximizing the formation energy in the size (in other words, solving the Eq. (42)), the critical size is given by

$$s_* = \frac{a^2}{4\Delta\mu^2}. \quad (43)$$

The nucleus with the critical size is characterized by the 50/50 probability of either growth or decay. The formation energy required for such critical nucleus is called the nucleation barrier and is given by

$$F_* = \frac{a^2}{4\Delta\mu}. \quad (44)$$

To summarize, this two-step procedure, namely maximization in s and minimization in x of the formation energy, corresponds to simultaneously solving the system of Eqs. (41) and (42).

Usually it is assumed that the surface energy of the ternary nucleus is effectively composition-independent (*Paper I*), (*Paper III*), [77], [94], [102], [103], i.e. $da/dx = 0$. This assumption is discussed in Section 4.2.1, while the influence of the surface energy term on the liquid-solid composition dependence is studied in *Paper II*. Assuming $da/dx = 0$, minimization of the nucleation barrier (Eq. (44)) in the solid composition x gives the relationship between the solid and liquid compositions:

$$\frac{\partial\Delta\mu}{\partial x} = 0. \quad (45)$$

Interestingly, Eq. (45) can be further reduced to the equality of the chemical potentials difference of the AD and BD pairs:

$$\Delta\mu_{AD} = \Delta\mu_{BD}. \quad (46)$$

Indeed, substituting the chemical potential difference and differentiating with respect to the solid composition, we obtain

$$\frac{\partial\Delta\mu}{\partial x} = \Delta\mu_{AD} - \Delta\mu_{BD} + \left(x \frac{\partial\Delta\mu_{AD}}{\partial x} + (1-x) \frac{\partial\Delta\mu_{BD}}{\partial x} \right). \quad (47)$$

The expression in the brackets equals to zero because of $\partial\Delta\mu_{AD}/\partial x = RT/x - 2(1-x)\omega_s$ and $\partial\Delta\mu_{BD}/\partial x = -RT/(1-x) + 2x\omega_s$. Eq. (46) is indeed true regardless of model. It is an effect of the Gibbs-Duhem equation.

Coming back to the formation energy, the solution to the system of Eq. (41) and (42) corresponds to finding of the saddle point of the formation energy surface (F, x, s) . To simplify the analysis, let's continue to consider the case of the composition-independent surface energy of the ternary nucleus ($da/dx = 0$). Figure 3.5 shows the energy landscape for $\text{In}_x\text{Ga}_{1-x}\text{As}$ alloy at $T = 450^\circ\text{C}$. It can be seen in the projection that the single saddle point appears at $x \approx 0.12$ and $s \approx 24$.

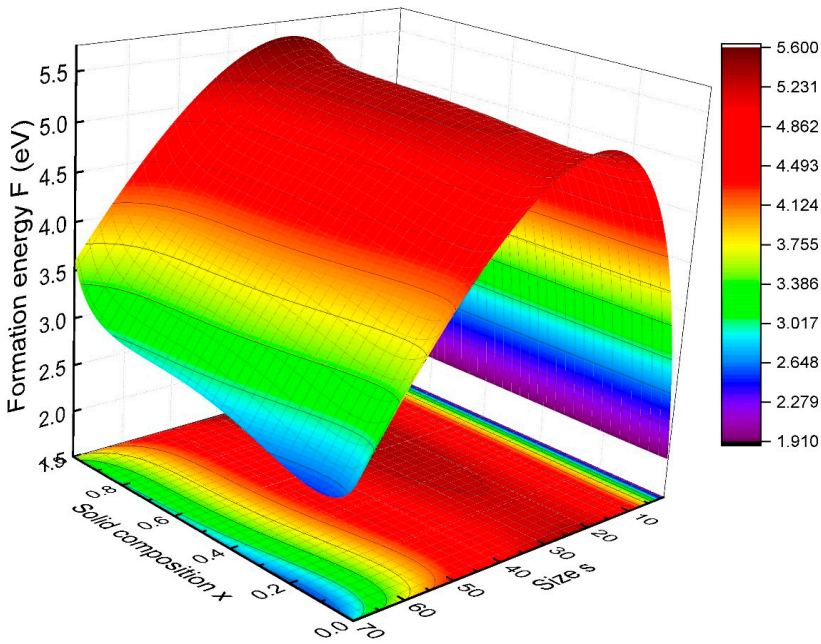


Figure 3.5. Three-dimensional plot and corresponding two-dimensional contour plot of the formation energy of the $\text{In}_x\text{Ga}_{1-x}\text{As}$ nucleus as a function of the solid composition and the nucleus size at fixed $y = 0.985$, $T = 450^\circ\text{C}$, $c_{As} = 0.02$ and $c_{Au} = 0.48$. The values of the rest of the parameters can be found in *Paper V*.

Usually, there is only one saddle point at each composition of the liquid particle. It shifts continuously over the solid composition (ranging from 0 to 1) with changing the liquid composition y from 0 to 1. However, for some of the material systems, two saddle points appear at a certain value of the liquid composition y and at temperatures lower the critical one. They have different solid compositions. Appearance of the second local minimum in the formation energy of the nucleus

and a jump of the saddle point from the region of low x to the one of high x with the critical case of the presence of two saddle points are presented in Figure 3.6.

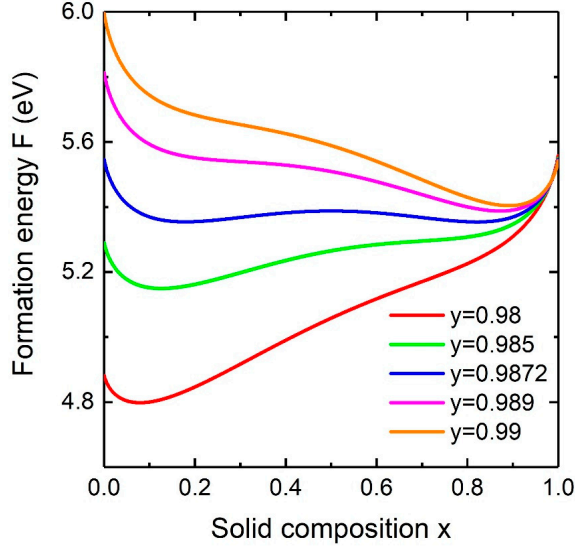


Figure 3.6. Formation energy versus the solid composition for $\text{In}_x\text{Ga}_{1-x}\text{As}$ alloy for different liquid compositions y .

It will be shown later that the described case is relevant for material systems with high value of the pseudo-binary interaction parameter. The distance between two saddle points is equal to the width of the miscibility gap.

The solution to the systems of Eq. (41) and (42) and its comprehensive analysis is presented in Section 4.2.1 and in *Paper I*. Modelling the chemical composition of self-catalyzed nanowires is presented in [103]. There it has shown that in the general case of self-catalyzed growth, the liquid-solid composition dependence is a three-parametric function, namely $(c_A + c_B)\omega_{AB}$, α and ω_s . It is reduced to the two-parametric function of α and ω_s if $|\Delta\mu_{AD}^0 - \Delta\mu_{BD}^0| \gg |\omega_{AB}|$ with $\Delta\mu_{AD}^0 = \mu_A^0 + \mu_D^0 - \mu_{AD}^0$ and $\Delta\mu_{BD}^0 = \mu_B^0 + \mu_D^0 - \mu_{BD}^0$. Finally, for the material systems with a small value of the pseudo-binary interaction parameter $\omega_s \approx 0$, the liquid-solid composition dependence can be further reduced to the one parametric function, namely to the Langmuir–McLean equation $x = \varepsilon y / (1 + (\varepsilon - 1)y)$ with $\varepsilon = e^\alpha$.

3.3.3 Incorporation model

The incorporation model is based on the balance between crystal growth and dissolution which are described by the attachment W^+ and detachment W^- rates.

The details can be found in the book [42]. Within homogeneous nucleation (i.e. the process which occurs in the absence of the “foreign” condensation center), the condensation or evaporation processes occur as a result of adding or subtracting the free monomer A_1 :

$$A_{i+1} = A_i + A_1. \quad (48)$$

Here A_i denotes the nucleus with i monomers. This process is schematically presented in Figure 3.7.

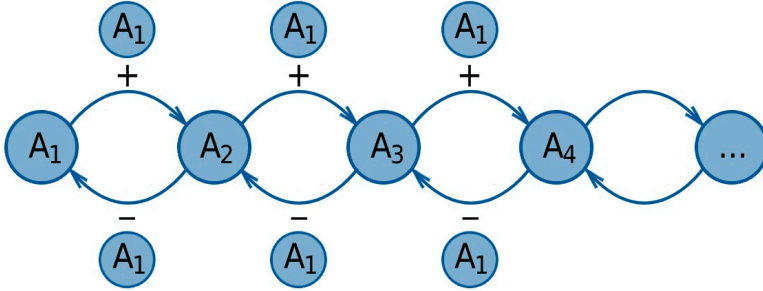


Figure 3.7. Schematic illustration of the reaction scheme for homogeneous nucleation.

The flux of monomers from the level $i - 1$ to i is given by

$$J_i = W_{i-1}^+ n_{i-1} - W_i^- n_i. \quad (49)$$

Here n_i is the concentration of nuclei containing i monomers. Considering the principle of detailed balance and the quasi-equilibrium distribution described by the Boltzmann distribution, the detachment rate can be expressed as

$$W_i^- = W_{i-1}^+ e^{F_i - F_{i-1}}. \quad (50)$$

Using the Taylor expansion $F_i - F_{i-1} = dF(i)/di - 1/2 d^2F(i)/di^2 + \dots$, Eq. (50) can be reduced to

$$W^-(i) = W^+(i) e^{\frac{dF}{di}}. \quad (51)$$

Considering the mononuclear mode and dropping the size dependence from the notation ($W^+(i) = W^+$), the incorporation rates of AD and BD species into the monolayer (the growing stable nucleus) defined as $dN_{AD}/dt = W_{AD}^+ - W_{AD}^-$ and $dN_{BD}/dt = W_{BD}^+ - W_{BD}^-$ are given by

$$\frac{dN_{AD}}{dt} = W_{AD} \left(1 - e^{\frac{dF}{dN_{AD}}} \right), \quad (52)$$

$$\frac{dN_{BD}}{dt} = W_{BD} \left(1 - e^{\frac{dF}{dN_{BD}}} \right). \quad (53)$$

Here the notation $W_{AD} = W_{AD}^+$ and $W_{BD} = W_{BD}^+$ is used. If the contribution of the surface energy in the formation energy is small, one may use $dF/dN_{AD} = -\Delta\mu_{AD}$ and $dF/dN_{BD} = -\Delta\mu_{BD}$. Then, it is clearly seen that the incorporation rate depends on the chemical potential difference of the corresponding pair. So, if the chemical potential difference is much larger than 1, the term in the brackets equals to 1 and the incorporation rate coincides with the attachment rate. Otherwise, the term in the brackets is very small and limits the incorporation rate. Next, the attachment rate is always proportional to the monomer concentration. This explains our assumption in *Paper III* that the attachment rate is proportional to the concentration of A or B and D elements in the droplet.

This is the basic idea of the incorporation model. Its analysis with application to nanowire growth is presented in *Paper III*, with a brief summary in Section 4.2.2.

3.3.4 Material balance model

As follows from its name, the central idea of this approach is the balance of the number of atoms in the droplet. Within the model, nanowire growth is considered as a dynamic continuous process without a nucleation step. Growth is described as a sink of the materials as a result of the nanowire elongation.

In the most general case, the change of the number of k atoms in the liquid particle (N_k^L) with time t is given by

$$\frac{dN_k^L}{dt} = \chi_k I_k^{dir} \pi R^2 + \chi_k I_k^{re} \pi R^2 + 2\pi R (j_k^+ - j_k^-) - \frac{2}{1 + \cos\beta} I_k^{des} \pi R^2 - \frac{\pi R^2}{\Omega_s} \frac{dL}{dt}. \quad (54)$$

Here, χ_k is the coefficient which describe the beam geometry in MBE and the cracking efficiency in MOVPE; I_k^{dir} , I_k^{re} and I_k^{des} are the direct atomic flux, the re-emitted flux and the desorption flux, respectively; j_k^+ and j_k^- are the diffusion flux to the droplet and the reverse diffusion flux; β is the contact angle; R is the nanowire radius; Ω_s is the volume per III-V pair in the solid and dL/dt is the nanowire elongation rate.

There are a number of simplifications, which help to find the solution. So, group V atoms are highly volatile and thus, do not diffuse along the nanowire. Therefore,

one can neglect its diffusion flux. On the other hand, group III atoms do not desorb from the droplet and nanowire sidewalls. Thus, its desorption and the re-emission flux can be neglected. The re-emission flux is considered to be proportional to the direct atomic flux [104]. Since the direct atomic flux, the re-emitted flux and the desorption flux are proportional to the droplet area, one might combine all of them introducing the effective flux I_k . Next, one may assume the absence of the reverse diffusion flux and use the approximation that the diffusion flux to the droplet is proportional to the effective flux and the diffusion length λ_k .

Considering growth of ternary $A_xB_{1-x}D$ nanowires and considering the assumptions discussed above, the material balance has the form

$$\frac{dN_A^L}{dt} = \chi_A I_A \pi R^2 + 2\varphi_A I_A \lambda_A R - x \frac{\pi R^2}{\Omega_s} \frac{dL}{dt}, \quad (55)$$

$$\frac{dN_B^L}{dt} = \chi_B I_B \pi R^2 + 2\varphi_B I_B \lambda_B R - (1-x) \frac{\pi R^2}{\Omega_s} \frac{dL}{dt}, \quad (56)$$

$$\frac{dN_D^L}{dt} = \chi_D I_D \pi R^2 - \frac{\pi R^2}{\Omega_s} \frac{dL}{dt}. \quad (57)$$

Here φ_k is a geometrical coefficient. Assuming that the number of each kind of atoms does not change with time and dividing Eq. (55) by Eq. (56), the solid composition can be obtained in the form of the one-parametric function:

$$x = \frac{1}{1 + K_{kin} \frac{1-z}{z}} \quad (58)$$

with the parameter

$$K_{kin} = \frac{\chi_B \pi R_{st} + 2\varphi_B \lambda_B}{\chi_A \pi R_{st} + 2\varphi_A \lambda_A}. \quad (59)$$

Here $z = I_A/(I_A + I_B)$ is the vapor composition. As seen from Eq. (59), increasing the nanowire radius, the parameter K_{kin} tends to 1 at fixed values of the diffusion length. Thus, according to this simple model, the solid composition should become closer to the vapor composition ($x \approx z$) for thicker nanowires. The comparison of the vapor-solid composition dependence calculated at $K_{kin} = 0.045$ and $K_{kin} = 0.011$ with the experimental data is presented in Figure 3.8.

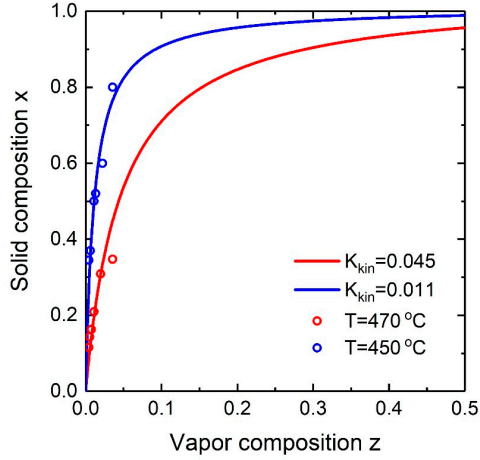


Figure 3.8. Theoretical (solid curves) and experimental (circles) vapor-solid composition dependence for $\text{In}_x\text{Ga}_{1-x}\text{Sb}$ nanowires for different temperatures. The experimental data are taken from [105].

More complicated kinetically-limited case has been considered by Dubrovskii in [106]. The solution can be presented in a similar way, namely

$$x = \frac{1}{1 + f(x)K_{kin} \frac{1-z}{z}} \quad (60)$$

with $f(x)$ being a complicated function of the solid composition. It has been shown that the solid composition differs from the vapor composition because of (i) the difference in diffusion fluxes of A and B atoms determined by the diffusion lengths and (ii) the asymmetry of the sinks.

It should be noted that the governing equations cannot be solved analytically in some cases. For example, in the case of very high density of nanowires when nanostructures compete for the atoms resulting in negligibly small diffusion flux from the substrate. Then, the diffusion flux is a complicated function of the nanowire length. In such cases, one may use numerical methods [22].

There are several advantages of the models based on the material balance. First, the final relationship links externally-controlled gas fluxes and the solid composition, which can be measured accurately. In other words, it allows us to skip the consideration of the liquid phase which composition is often unknown. Second, the material balance model can be used to describe the nanowire growth rate and morphology. For example, the morphology of GaP nanowires as a function of III/V flux ratio and pitch has been studied in [90]. In total, growing GaP nanowires on a Si substrate by gas source molecular beam epitaxy, we studied experimentally and fitted 25 different configurations (5 values of the flux ratio \times 5 values of the pitch). It has been shown that the key parameter which governs the nanowire morphology

is the flux ratio. Moreover, there is a weak dependence on the distance between nanowires (pitch). So, increasing of the V/III ratio leads to the transition from outward tapered, which is the case of regular unlimited growth to straight and ultimately sharpened nanowires in the so called self-focusing regime. The stable radius at high flux ratio is very small: it is possible to achieve a radius of 12 nm.

3.4 Nanowire crystal structure

In addition to the composition tuning, one may control the crystal phase of nanowires. So, nanowires of some of the compounds adopting the cubic zinc blende (ZB) crystal structure in bulk, have turned out to form hexagonal wurtzite (WZ) crystal phase. This phenomenon being a topic of comprehensive research is called polytypism. A classic example is GaAs which bulk energy (or, cohesive energy) difference between the two crystal phases equal to 24 meV per III-V pair [107]. GaAs nanowires composed of WZ, ZB or modulated crystal structures have been grown [88].

The ZB and WZ crystal structures are schematically presented in Figure 3.9. The difference between them involves the stacking sequence of close packed planes. The ZB crystal structure consists of two interpenetrating face center cubic lattices with cations on one lattice and anions on the other lattice, where one of the lattices is shifted towards $1/4$ of the distance along the body diagonal of the unit cell. The WZ crystal structure is a hexagonal close-packed structure where each atom forms four bonds. Such difference in atomic arrangements in the ZB and WZ crystals results in a difference of their band structure and, thus, electronic properties. On the one hand, the ability of crystal phase control gives some additional freedom in tuning the physical properties. On the other hand, such control is impossible without the understanding gained by fundamental studies of the nanowire crystal structure coupled with experimental work. So, incorrectly chosen conditions or the change of growth conditions can lead to formation of a nanowire which may combine different crystal structures.

During growth of ZB nanowires along $[\bar{1}\bar{1}\bar{1}]$, rotational twins might occur. This kind of twinning leads to a zigzag morphology of ZB nanowires, frequently observed in experiments [108].

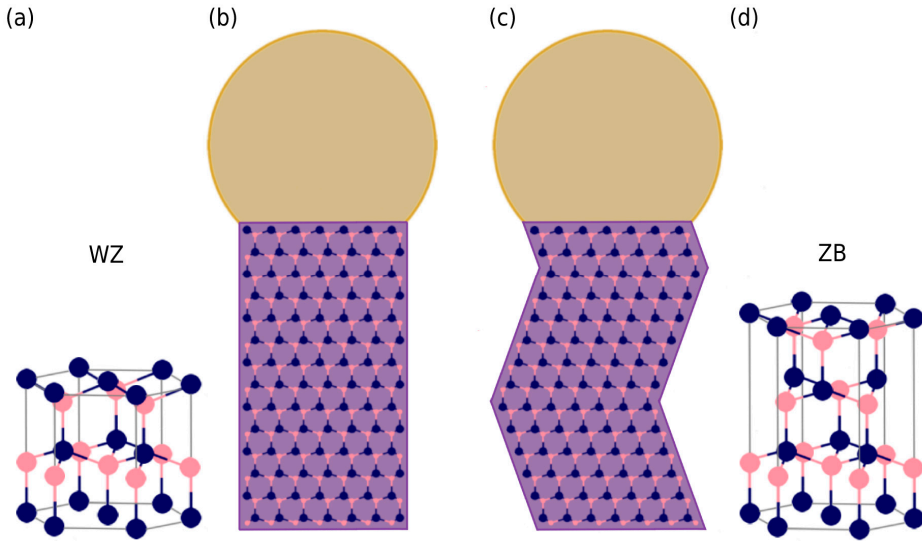


Figure 3.9. WZ (a) and ZB (d) crystal structures and schematic illustration of WZ (b) and ZB with twins (c) nanowires.

One of the first explanations of the ZB/WZ polytypism in nanowires has been given by Glas in the paper [56] with the telling name “Why does wurtzite form in nanowires of III-V zinc blende semiconductors?”. The idea is simple and it has been used for our investigations. It lies on the comparison of the probabilities of the formation of nuclei which have the ZB or WZ crystal structure at the triple phase line or in the center of the liquid-solid interface. According to calculations, the formation of WZ crystal phase can be energetically favourable at high liquid supersaturation.

Almost at the same time, a more detailed study was presented by Dubrovskii [109]. The transformation from the cubic to hexagonal crystal phase is described as a function of the liquid supersaturation and the material constants. To concluding, the selection of crystal structure during growth is defined by the chemical potentials and depends on the V/III flux ratio and the contact angle.

Modelling of the crystal structure of ternary nanowires nucleating from quaternary liquid melts, including the calculation procedure and the effect of the contact angle, the solid composition and temperature on the formation probabilities, is presented in *Paper V*. The obtained results are summarized in Section 4.3. In the *Paper V* the probabilities of the formation of the ZB and WZ structures have been calculated. Despite the fact that several parameters are still unknown, *Paper V* is a useful tool for modelling and understanding the crystal phase selection in ternary NWs.

4 Nanowire Growth Modelling and Results

This chapter focuses on summarizing my results on nanowire growth modelling. The limitations which arise from the assumptions made for modelling are presented in Section 4.1. After that, the composition of ternary nanowires nucleating from quaternary liquid melt is discussed in details in Section 4.2. It is split into three parts. The first one (Section 4.2.1) is devoted to the nucleation-limited growth regime. Here an analytical approach for understanding and tuning the composition in ternary III-V semiconductor nanowires is given. The shape of the liquid-solid composition dependence is explained and it is shown how it changes with the model parameters such as temperature, Au concentration and total concentration of group V elements. In the last subchapter, we show how the surface energy influences the liquid-solid composition dependence and the miscibility gap. The second part (Section 4.2.2) describes the nanowire composition as a combination of nucleation-limited and kinetically defined composition dependencies, utilizing the incorporation model. We discuss the thermodynamics and kinetics in the formation of ternary III-V nanowires and simulate the evolution of the nucleus composition during vapor-liquid-solid growth. Moreover, it is noted that high supersaturation may lead to miscibility gap suppression. In the third part (Section 4.2.3), the theoretical results are compared with the experimental liquid-solid composition dependence. In Section 4.3 we outline the thermodynamic modelling of crystal phase of ternary III-V nanowires and determine the growth conditions under which the formation of wurtzite (or zinc blende) nanowires is possible.

The main idea of this chapter is to highlight the main theoretical results presented in the papers and to concoct new interpretations and explanations of some of the trends which have been missed in the papers.

4.1 Assumptions and limitations

To explain the properties of the grown nanowires, one should consider movement of semiconductor materials from the source to the substrate, precursor decomposition in the case of MOVPE, possible homogeneous and heterogeneous

reactions in the chamber, a large number of elementary processes on the surface, nucleation and growth of a monolayer. Thus, some simplifications are needed to study the phenomenon, explain the observations, and find out the main tendencies.

Several assumptions have been used to describe the composition and crystal phase of ternary III-V nanowires:

- (i) First of all, classical nucleation theory is used as a theoretical foundation of the nucleation-limited model. It has its shortcomings such as the capillarity approximation [110], [111], [112] treating molecular clusters as macroscopic objects. Thus, there could be cases where classical nucleation theory fails. For example, the nucleation rate of crystalline monolayers might be overestimated [113]. Usually, such errors can be attributed to the smallest clusters and more sophisticated methods are needed such as consideration of quantum corrections [114], [115] or utilizing Monte Carlo simulations [44]. This means that the size of the critical nuclei should be relatively large. On the other side, classical nucleation theory has been tested in great detail and is widely used for description of the process of nucleation.
- (ii) Within the nucleation model, the calculated liquid-solid composition dependence and probabilities of cubic and hexagonal phase formation are originally attributed to the critical nucleus. In order to extend this approach to nanowires, one should assume that its composition does not change during monolayer completion. This is what is called the nucleation-limited regime.
- (iii) It is well known that some of the parameters of nanoscale particles are size-dependent. One of the examples is the Gibbs-Thomson effect [116], which involves an increase of the equilibrium pressure in the liquid particle and its chemical potential due to the surface curvature. Such size-dependent effects are not considered which limits the applicability of the model: the radius of the liquid particles should not be smaller than about 15 nm.
- (iv) Components in the liquid droplets are treated as homogeneously distributed. However, the liquid particle might be segregated [117]. Concentration of group V elements is considered to be composition independent. Moreover, it is assumed to be constant during growth while in reality there are concentration fluctuations [118].
- (v) Within the incorporation model, the attachment rates are proportional to the corresponding concentration of A or B and D elements in the liquid particle. This means that application of the model might be problematic in some extreme cases. Let's assume the case when the attachment rate of one of the components is the rate-limiting step. Then,

doubling the concentration of the other component should not increase the overall growth rate, which doesn't follow from the model. However, this assumption allowed us to model real experimental data.

- (vi) Within modelling of nanowire crystal structure, the liquid-solid surface energy is considered to be independent of the Au concentration. In a theoretical study on Au-catalyzed GaAs nanowires [119], values of the liquid-solid surface energy for a pure Ga droplet and for the case when the liquid particle consists mainly of gold ($c_{Ga} = 0.2$) differ by one order of magnitude.
- (vii) The initial stage of nanowire growth is not considered. The analysis is relevant for nanowires with a non-zero length. Thus, for example, the influence of the substrate on the growth process is ignored.
- (viii) Finally, one should remember that there is the minimum uncertainty in the values of specific surface energies and thermodynamic interaction parameters. Moreover, the surface energies depend on the orientation. There are no experimental data for the concentration of group V elements in the liquid nanoparticles.

To the best of my knowledge, the nucleation limited model might be used if conditions are close to equilibrium and supersaturation is low. Otherwise one should use the model based on incorporation rates. This would explain the fact that the miscibility gap is not observed during growth of nanowires using MBE or MOVPE.

The following sections present an account of developed theoretical models for description of different aspects of nanowire growth and nucleation. Its analytical nature allows one to study the nucleation and growth process varying the model parameters in order to find the most crucial and main tendencies which can be used later for optimization of growth conditions.

4.2 Composition of ternary nanowires

Many ternary nanowire-based applications arise from the possibility to tune the composition of multicomponent III-V nanowires, which enables tailoring their properties. A crucial step in the device fabrication is composition control because the compound concentrations in an alloy determine the bandgap and operating wavelength of such optoelectronic devices. Among other reviews [67], [68], the state-of-the-art research progresses on composition tuning in ternary III-V nanowires is summarized in our review paper "Assembling your nanowire: an overview of composition tuning in ternary III-V nanowires" [66]. In this overview we focus mainly on experimental studies and briefly discuss applications of each materials system. The literature on composition control in III-V nanowire materials

systems has been divided into four groups, namely growth of Au-catalyzed and self-catalyzed nanowires via vapor-liquid-solid mechanism and vapor-solid-solid growth of nanowire shells and catalyst free nanowires. We limited ourselves to III-V semiconductor materials and studied ternary $\text{III}_x\text{III}_{1-x}\text{V}$ nanowires (AlGaAs, AlGaP, AlInP, InGaAs, GaInP and InGaSb) and $\text{III}_x\text{V}_x\text{V}_{1-x}$ nanowires (InAsP, InAsSb, InPSb, GaAsP, GaAsSb and GaSbP). It has been shown that material systems such as GaAsSb, InAsSb, InGaAs and GaInP are well studied. However, there is a lack of data on composition tuning in the GaSbP, InSbP, AlInP and AlGaP systems. The composition of ternary III-V nanowires with the exception of Sb-based material systems can be controlled over a wide range by tuning the vapor composition. The Sb surfactant effect leads to non-uniform morphology and strong tapering, and requires more sophisticated growth methods.

4.2.1 Nucleation-limited composition

Based on the observations on vapor-liquid-solid nanowire growth [9], one may conclude that it occurs in the layer by layer mononuclear mode with the formation of a small nucleus. This layer-by-layer growth follows from the fact that the time between two nucleation events is greater than the time to compete a monolayer under regular MOVPE and MBE growth conditions. To highlight, the nucleation rate is entirely controlled by the height of the nucleation barrier in the nucleation model. So, considering the formation of $\text{A}_x\text{B}_{1-x}\text{D}$ nucleus from a quaternary liquid particle containing A, B, D, and U, where U is a solvent, the composition and size of the critical nucleus can be found from the simultaneous solutions of the equations $\partial F/\partial x = 0$ and $\partial F/\partial s = 0$.

With the exception of the final subchapter 4.2.1.6 based on *Paper II*, in my calculations the surface energy of the ternary nucleus is assumed to be composition independent. To be more specific, it implies the segregation of the component with the lower surface energy to the surface. This means that irrespective of the composition of the ternary nucleus, its surface energy equals the one of the components with the lower surface energy. This is questionable but a commonly accepted assumption originally used by Wilemskii [120] for description of liquids nucleating from vapor. In any case, it allows us to reduce the system of partial differential equations to the equation of $\partial\Delta\mu/\partial x = 0$ or, as it has been already shown, to the equation of $\Delta\mu_{AD} = \Delta\mu_{BD}$.

Substituting the chemical potentials and simplifying, a relation between the liquid and solid compositions was found. To analyse the relationship, it can be rewritten as

$$y = \frac{1}{1 + \frac{(1-x)}{x} e^{b(y)+g(x,\omega_s)}}. \quad (61)$$

Here $g(x, \omega_s)$ is a function of the solid composition and the pseudobinary interaction parameter. In the case of composition independent pseudobinary interaction parameter $g(x, \omega_s) = 2\omega_s(x - 1/2)/(RT)$. The function $b(y)$ is complicated and depends on the concentrations of all the elements in the liquid particle and interaction parameters.

Using the developed analytical approach, the composition tuning in Au-catalyzed and self-catalyzed $\text{In}_x\text{Ga}_{1-x}\text{As}$, $\text{Al}_x\text{Ga}_{1-x}\text{As}$, $\text{In}_x\text{Ga}_{1-x}\text{Sb}$, $\text{InSb}_x\text{As}_{1-x}$ (*Paper I*) nanowires has been considered and analysed. It has been demonstrated that the solid composition can be varied in a wide range by tuning the liquid composition at relevant growth temperatures. The exceptions are material systems with high pseudobinary interaction parameter, ω_s , such as In-Ga-As and In-Sb-As ones. In such materials systems the nucleation-limited liquid-solid composition dependence contains the miscibility gap within which the formation of a homogeneous ternary solid solution is thermodynamically forbidden. Such miscibility gap appears in the ternary alloys with $\omega_s > 2RT$.

4.2.1.1 Shape of the liquid-solid composition dependence

The simplified form of the liquid-solid composition dependence (Eq. (61)) is convenient because one may consider the dependence separately, namely the one consisting $b(y)$ (putting $\omega_s = 0$) and the one which depends on the pseudobinary interaction parameter (putting $b(y) = 0$). As it will be shown later in this subchapter, the liquid composition y is very close to 0 or 1 (depending on the notation in $\text{A}_x\text{B}_{1-x}\text{D}$ alloy) in the almost entire range of the solid composition for the majority of material systems. Then, one might put the liquid composition y in the exponent to one or zero and consider b as a constant with the parameters of temperature and concentrations of the D and U components. This results in a closed form approximation (Eqs. (11) and (12) in *Paper I*). Comparison of the numerical exact and approximate solutions showed good agreement (see Figure 8 in *Paper I*) with the obvious exception of the intermediate liquid compositions ($y \approx 0.5$). The liquid-solid composition dependences being the solutions of $y = 1/(1 + e^b(1-x)/x)$ and $y = 1/(1 + e^{2\omega_s(x-1/2)/(RT)}(1-x)/x)$ are presented in Figure 4.1.

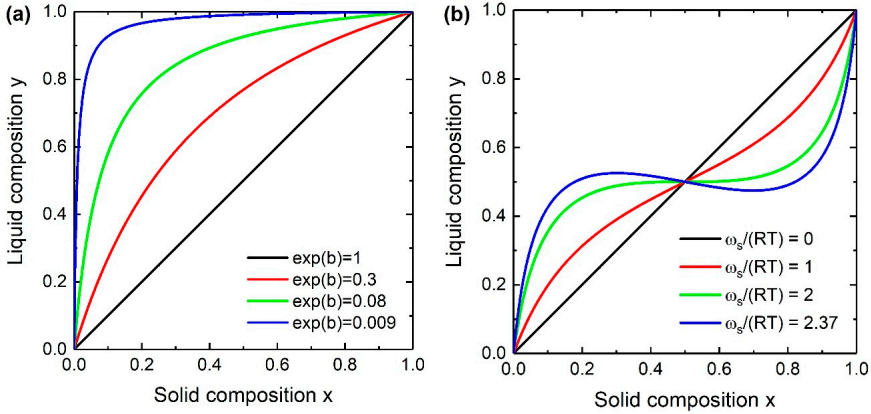


Figure 4.1. The liquid-solid composition dependences being the solutions of $y = 1/(1 + e^b (1-x)/x)$ for different values of the constant b (a) and $y = 1/(1 + e^{2\omega_s(x-1/2)/(RT)} (1-x)/x)$ for different values of ω_s (b).

As seen from Figure 4.1, decreasing the constant b the curve shifts to one of the corners (see Figure 4.1a) while the s-shape of the curve arises from the term consisting the pseudobinary interaction parameter (see Figure 4.1b). This explains the shape of the liquid-solid composition dependence, namely its very steep and s-shaped behaviour. The critical value of the pseudobinary interaction parameter at which the miscibility gap arises is $\omega_s = 2RT$. The value of $\exp(b) = 0.009$ corresponds to the one calculated for Au-catalyzed $\text{In}_x\text{Ga}_{1-x}\text{As}$ nanowires at $T = 450$ °C, $c_{\text{Au}} = 0.3$ and $c_{\text{As}} = 0.01$. At this temperature $\omega_s/(RT) = 2.37$. So the combination of the blue curves gives the curve calculated at $T = 450$ °C and presented in Figure 3 of *Paper I*.

The difference of the chemical potentials of pure elements and compounds $\Delta\mu^0 = \Delta\mu_{AD}^0 - \Delta\mu_{BD}^0 = (\mu_A^0 - \mu_{AD}^0) - (\mu_B^0 - \mu_{BD}^0)$ has the largest contribution to the constant b . So, under the conditions used for Figure 4.1, $b \approx -4.74$ and $\Delta\mu^0/(RT) \approx -4.43$. The rest is the contribution from the binary and ternary interactions in the liquid. In the case of self-catalyzed growth, apart from $\Delta\mu^0$ the highest impact has the In-Ga interaction parameter in the liquid (see Figure 4.2).

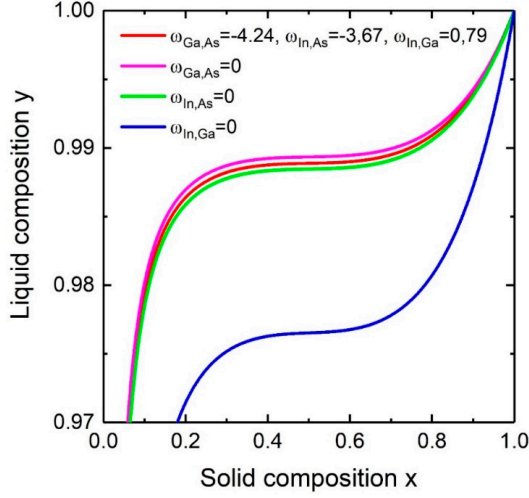


Figure 4.2. Liquid-solid composition dependence for $\text{In}_x\text{Ga}_{1-x}\text{As}$ alloy at fixed $T = 550\text{ }^\circ\text{C}$, $c_{\text{Au}} = 0$ and $c_{\text{As}} = 0.02$ with different interaction parameters in the liquid (the values are divided by RT).

High value of $\Delta\mu^0$ (and consequently, the constant b) obtained for the all of the considered material systems results in the necessity of the predominance of one of the components (A or B) in the droplet to tune the solid composition in a wide range. In other words, it explains that $y \approx 1$ or $y \approx 0$ for $0 < x < 1$.

4.2.1.2 Effect of temperature on the liquid-solid composition dependence

As mentioned above, considering the nucleation model with the compositional independent surface energy term, the only parameter which determines the miscibility gap is the pseudobinary interaction parameter. Being temperature dependent, it is natural to expect that the miscibility gap should also change with temperature. Figure 4.3a shows InAs-GaAs interaction parameter $\omega_{\text{InAs-GaAs}} = 2(9849.4 - 3.758465T)$ versus temperature. As seen, the pseudobinary interaction parameter decreases with temperature and $\omega_{\text{InAs-GaAs}}/(RT) = 2$ at the critical temperature of $T = 543\text{ }^\circ\text{C}$. The liquid-solid composition dependence for InGaAs alloy for different temperatures and Au concentrations at fixed $c_{\text{As}} = 0.01$ is presented in Figure 4.3b. As expected, the miscibility gap, which doesn't depend on the Au concentration (compare the red and light blue curves), shrinks with temperature and disappears at $T = 543\text{ }^\circ\text{C}$.

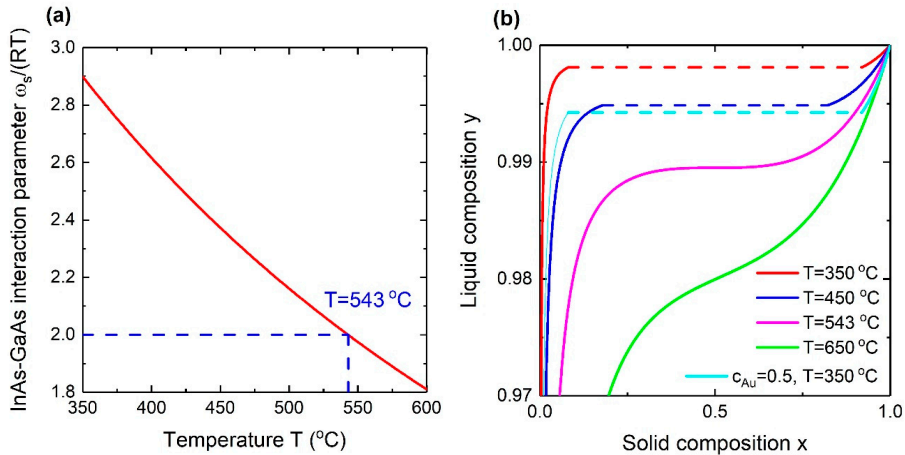


Figure 4.3. InAs-GaAs interaction parameter versus temperature (a) and the liquid-solid composition dependence for InGaAs alloy for different temperatures and Au concentrations at fixed $c_{As} = 0.01$ (b). Light blue corresponds to Au-catalyzed growth ($c_{Au} = 0.5$) and the rest corresponds to self-catalyzed growth ($c_{Au} = 0$). The dashed parts of the curves correspond to the miscibility gap.

4.2.1.3 Effect of concentration of group V elements on the liquid-solid composition dependence

It has been found that the concentration of group V elements has no visible influence on the liquid-solid composition dependence within the nucleation model. Thus, irrespective of the Au concentration, the curves calculated for $In_xGa_{1-x}As$ alloy at the As concentrations with an order-of-magnitude difference coincide (see Figure 4.4). This is in contrast to the incorporation model where the concentration of group V elements plays an essential role in the liquid-solid composition dependence (see *Paper III*).

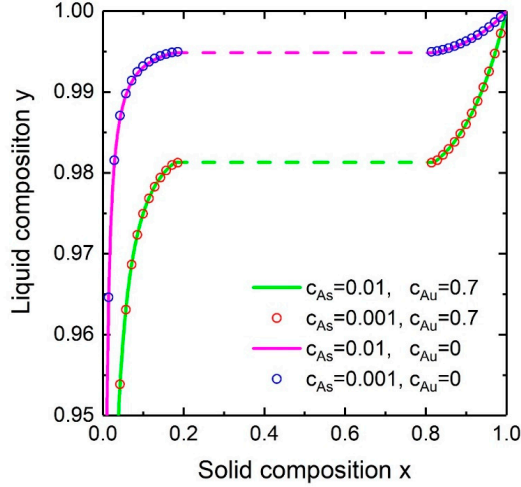


Figure 4.4. Liquid-solid composition dependence for $\text{In}_x\text{Ga}_{1-x}\text{As}$ alloy at fixed $T = 450$ °C for different As concentrations of $c_{\text{As}} = 0.01$ and $c_{\text{As}} = 0.001$ and Au concentrations of $c_{\text{Au}} = 0$ and $c_{\text{Au}} = 0.7$.

4.2.1.4 Account of ternary and binary composition-dependent interaction parameters

One of the advantages of the presented model is the account of a large number of different interaction parameters including ternary and binary composition-dependent and pseudobinary composition-dependent interaction parameters. Their impact on the liquid-solid composition dependence on the example of $\text{In}_x\text{Ga}_{1-x}\text{As}$ alloy can be assessed from Figure 4.5. As seen, account of the composition-dependent binary interaction parameters and ternary interaction parameters results in shifting of the liquid-solid composition dependence in different directions (compare the green and blue curves with the magenta one as the reference curve). Thus, either one should ignore all of them except of the binary composition-independent interaction parameters (ω_{ij}^0), either take into account all the interactions parameters. The difference between these two (the magenta and red curves, correspondingly) is relatively large. So, the difference between the liquid composition values which corresponds to the miscibility gap is about $\Delta y = 0.9967 - 0.9931 \approx 0.004$. In the terms of temperature, to obtain the same Δy one need to change temperature by roughly 90 °C under the same conditions. Therefore, one might conclude that it is important to consider all of the interaction parameters. Indeed, using only the full set of the optimized interaction parameters, one may reconstruct the phase diagram of the corresponding material system. Once one neglects some of the interaction parameters, the accuracy decreases.

As for the composition-dependent pseudobinary interaction parameter, its account leads to the shifted and asymmetric shape of the miscibility gap (see Figure 10 in *Paper I*).

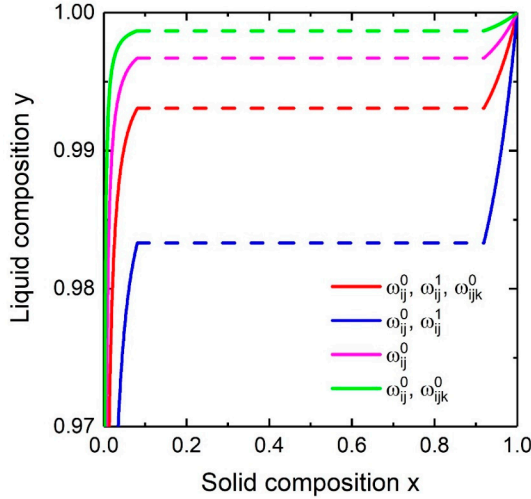


Figure 4.5. Liquid-solid composition dependence for $\text{In}_x\text{Ga}_{1-x}\text{As}$ alloy at fixed $T = 350^\circ\text{C}$, $c_{\text{Au}} = 0.6$, $c_{\text{As}} = 0.01$ calculated at different types of interaction parameters: all parameters correspond to the red curve, except of the ternary interaction parameters is the blue curve, except of the composition-dependent binary interaction parameters is the green curve, composition-dependent binary interaction parameters is the magenta curve.

4.2.1.5 Effect of Au concentration on the liquid-solid composition dependence

Summarizing the effect of the Au concentration on the liquid-solid composition dependence, it has been found that increasing the Au concentration results in an increase of indium in $\text{In}_x\text{Ga}_{1-x}\text{As}$ and $\text{In}_x\text{Ga}_{1-x}\text{Sb}$ alloys, gallium in $\text{Al}_x\text{Ga}_{1-x}\text{As}$ alloy, arsenic in $\text{InSb}_x\text{As}_{1-x}$ alloy at fixed ratio of the concentrations of the A and B components in the liquid.

4.2.1.6 Effect of the surface energy on the liquid-solid composition dependence

As mentioned above, a significant simplification in modelling of nanowire composition and a relatively simple form of the governing equation of $\Delta\mu_{AD}/\Delta\mu_{BD} = 1$ have been achieved due to the assumption of the independence of the surface energy term on the nucleus composition. To analyse the influence of the surface energy of the ternary nucleus on the liquid-solid composition dependence including the miscibility gap, one should consider the full set of partial differential equations $\partial F/\partial x = 0$ and $\partial F/\partial s = 0$ without any simplifications. The solution in this case and its discussion are presented in *Paper II*. The important intermediate solution (see Eq. (5) in *Paper II*) takes the form

$$\frac{\Delta\mu_{AD}}{\Delta\mu_{BD}} = 1 + f\left(\frac{da}{dx}, x\right). \quad (62)$$

This equation shows in a clear way the difference from the previous solution. So, the two chemical potential differences, corresponding to the AD and BD pairs, are not equal: there is an addition of $f(da/dx, x)$. The modification of the liquid-solid composition dependence depends on the values of da/dx and x . In turn, da/dx is determined by the model which one uses to describe the relation between the surface energy of the ternary nucleus and the ones of binary compounds. Depending on the form, it could be

- (i) a constant being the surface energy of one of the binary compounds (the one with the lower surface energy) corresponding the Wilemski approach;
- (ii) a linear combination of the surface energies of the binary compounds according to the Vegard's law;
- (iii) intermediate cases between (i) and (ii);
- (iv) a convex function of the surface energies of the binary compounds, corresponding to Vegard's law with a bowing parameter (a second degree correction term).

Clearly, the contribution of the surface energy term in the formation energy is determined by the ratio of the surface energies of the binary compounds (absolute values) and the path which links them (the model).

In any case, the solid composition depends on the liquid composition y (as in the previous case), the concentration of the D component c_D and the ratio of the surface energies of the binary compounds through the term da/dx .

Summarizing the obtained results, it has been shown that high value of the surface energy ratio might lead to suppression of the miscibility gap (Figure 4a in *Paper II*). Calculating the liquid-solid composition dependence of $\text{In}_x\text{Ga}_{1-x}\text{As}$ nanowires, the surface energy contribution is small and almost does not change the miscibility gap because of the similar values of InAs and GaAs surface energy terms. However, within the convex model the miscibility gap is completely suppressed if the ratio of InAs and GaAs surface energy terms is 1.15 or larger.

4.2.2 Incorporation-limited composition

At this stage, there are no indications that at the vapor-liquid-solid growth of $\text{In}_x\text{Ga}_{1-x}\text{As}$ nanowires, the binary compounds segregate in the solid nanowire. To explain this, thermodynamic and kinetic approaches have been combined within the incorporation model. The solid composition is determined by the numbers of the

incorporated AD and BD pairs $x = N_{AD}/(N_{AD} + N_{BD})$, and thus their incorporation rates into the solid. To remind, the governing equations which describe the incorporation rates of the AD and BD pairs are $dN_{AD}/dt = W_{AD}(1 - e^{-\Delta\mu_{AD}})$ and $dN_{BD}/dt = W_{BD}(1 - e^{-\Delta\mu_{BD}})$ ignoring the contribution of the surface energy term in the formation energy (*Paper III*).

The formation of nanowires has been considered as a two-step process. The two processes are nucleation leading to formation of a critical nucleus and growth according to equations which describe the incorporation rates. The critical nucleus has the nucleation limited composition and it will tend to the steady state composition which is determined by kinetics during the growth. Such a model allows us to study the evolution of the solid composition of ternary nanowires grown via the vapor-liquid-solid mechanism. So, the composition of ternary nanowires can be presented as a linear combination of the nucleation-limited solid composition and the kinetic one (see Eq. (12) and Figure 5 in *Paper III*). The ratio of the critical nucleus size and the size of the evolving nucleus defines the evolution rate.

It should be noted that within the model, the attachment rates W_{AD} and W_{BD} are functions the nucleus size, $f(s)$, which could, in principle, be any function of the size. For example, one may assume the attachment rate to be proportional to the nucleus perimeter, so that $f(s) \sim \sqrt{s}$. Or, one can consider the more realistic case, which might be relevant for nanowires when $f(s)$ is a non-monotonic function: it increases from zero, reaches a maximum value and then gradually decreases to zero again. This is because the effective “growing part” of the nucleus perimeter (the perimeter with the exception of the part which is in contact with the vapor) increases first and then decreases. In other words, the incorporation rate could be close to zero for small nuclei ($s \approx s^*$) so that the critical nucleus has a small growth rate. However, it should be small for the both AD and BD pairs and since we are interested in the ratio of the incorporation rates only, this size dependent function $f(s)$ vanishes.

In addition to the evolution of the nucleus composition, the steady state composition $x_s = dN_{AD}/dt/(dN_{AD}/dt + dN_{BD}/dt)$ has been studied. Importantly, it is determined by the concentration of group V elements (see Figure 3 in *Paper III*). So, under conditions which provide high supersaturation, the miscibility gap can be suppressed completely in the steady-state growth regime. As for the effect of temperature and Au concentration (or U component) on the liquid-solid composition dependence, it is the same as in the nucleation-limited growth regime.

Finally, based on calculations of the chemical potential difference, the compositional limit which is observed in a ternary alloy containing antimony has been explained. So, low Sb concentration in the droplet leads to larger area where the chemical potential difference is negative and nucleation is not energetically favourable (which means no NW growth).

4.2.3 Comparison theory and *in-situ* analysis

The confirmation of the obtained theoretical results is possible only when the measurements are carried out during nanowire growth. On the one hand, the *in-situ* technique provides unique information that cannot be gleaned by studying conventional MOVPE and MBE growth of nanowires, such as the nucleation statistics [118], the geometry and dynamics of the interfacial step flow [9], the relationship between the nanoparticle and ternary nanowire (*Paper IV*). On the other hand, growth of nanowires in a transmission electron microscope is very specific. First, the total pressure used for MOVPE nanowire growth is too high for TEM and should be reduced. Second, a SiN_x grid is used instead of a conventional substrate, e.g., Si. This results in a decrease of the precursor decomposition rate. In addition, there is no diffusion of the group III element from the substrate, which plays an essential role during conventional MOVPE and MBE growth of nanowires. Moreover, the diffusion flux from the nanowire sidewalls to the droplet depends on the nanowire length for short nanowires. In the case of MOVPE growth, high ratio of the group V precursor flux to the group III precursor (or, V/III ratio) is needed [75]. In the case of growth of nanowires using transmission electron microscopy, the V/III ratio seem to be even more important. So, V/III ratios of order of 1000 is needed to ensure both vapor-liquid condensation and liquid–solid crystallization [121]. Such high value might be explained by low efficiency of the precursor decomposition in absence of the substrate and/or no diffusion of the group III element from the substrate. Summarizing, the findings obtained by *in-situ* techniques might help us to understand the general tendencies and describe the underlying mechanism. At the same time, some of the results cannot be directly applied to MOVPE growth.

Recently, growth of binary nanowires has been studied using transmission electron microscopy. For example, in paper [122], the *in-situ* technique is used to study the composition of the liquid droplet. It has been shown that the Ga content in the liquid particle increases with both temperature and Ga precursor flux. Moreover, the growth rate increases with Ga precursor flux, saturating at very high Ga precursor flux. The saturation of the growth rate at very high Ga precursor flux is explained by a gradual transition from the Ga-limited toward the As-limited growth. The precursors TMGa and AsH₃ were used. Growing GaAs nanowires at low V/III ratio (i.e. at low AsH₃ flow), both incubation and layer growth are limited by As. At high AsH₃ flow, growth is limited by Ga (with an intermediate case when growth is determined by both Ga and As flows).

In the *Paper IV*, an environmental transmission electron microscope is used to study growth of In_xGa_{1-x}As nanowires. In particular, the correlation between the compositions of the liquid droplet and ternary nanowires has been obtained. Considering the complex behaviour of the liquid-solid composition dependence, it is impossible to model the experimental data applying the existing models without

a drastic improvement. So, the liquid-solid composition dependence can be divided roughly into three parts, namely a steep slope section at small values of the solid composition ($x < 0.2$), an almost horizontal line in the middle ($0.2 < x < 0.8$) and a shallow slope section at high values of the solid composition ($x > 0.8$). This excludes a possible application of the kinetic models based on the material balance [106]. Moreover, too rapid transition of the $y(x)$ curve from an almost vertical line to an almost horizontal line makes some advanced kinetic models [77] and [102] inapplicable. The nucleation-based model (*Paper I*), [103] predicted the shape and the In-rich droplet is not flexible enough: the position of the $y(x)$ curve is determined primarily by the In-Ga interaction parameter in the liquid and can be slightly changed by the Au concentration and growth temperature (*Paper I*), which are known and fixed. Moreover, within the model, at such low temperature there should be a miscibility gap where the formation of a homogeneous solid solution is thermodynamically forbidden (*Paper I*). However, as shown before, the surface energy might suppress the miscibility gap in nanostructured ternary solid solutions (*Paper II*).

To explain the obtained results, we used the incorporation model (*Paper III*) taking into account the surface energy (*Paper II*). In other words, growth of Au-catalyzed $\text{In}_x\text{Ga}_{1-x}\text{As}$ nanowires occurs as a result of the incorporation of InAs and GaAs pairs into the growing nucleus with the incorporation rates of $dN_{AD}/dt = W_{AD}(1 - \exp(-\Delta\mu_{AD} + F_{AD}^{surf}))$ and $dN_{BD}/dt = W_{BD}(1 - \exp(-\Delta\mu_{BD} + F_{BD}^{surf}))$, respectively. The surface energy term F^{surf} is the derivative of the second term of the nucleus formation energy over the respective number of pairs. It seems the incorporation model describes well enough the experimental data and the surface energy plays a significant role in the formation of a monolayer. However, one should remember that the data represents the set of experiments collected on several nanowires which Au content in the droplet might differ. More accurate consideration would help to reduce the number of parameters.

4.3 Crystal structure of InGaAs nanowires

While polytypism in binary III-V semiconductor nanostructures is well experimentally studied and understood, there is no theoretical description of this phenomenon in ternary alloys. It is of paramount importance for highly efficient optoelectronic devices based on ternary nanowires to obtain uniform crystal structure. The transformation from cubic to hexagonal crystal phase has been studied in *Paper V* on the example of $\text{In}_x\text{Ga}_{1-x}\text{As}$ nanowires being well known to exhibit the zinc blende or the wurtzite crystal structure.

The idea of modelling of the crystal structure formation is the following. First of all, to describe the case of nanowire growth, four configurations should be considered:

two different crystal phases and two possible sites where nucleation may occur, namely at the triple line (*TPL*) and in the center of the liquid-solid interface (*C*), so that $k = TPL, C$. To calculate the formation probabilities for cubic and hexagonal crystal phases, one should compare the corresponding nucleation rates being $J_{ZB,k} = A_k J_0 \exp(-F_{ZB,k}^*/(RT))$ and $J_{WZ,k} = A_k J_0 \exp(-F_{WZ,k}^*/(RT))$. The nucleation barriers $F_{ZB,k}^*$ and $F_{WZ,k}^*$ are functions of the corresponding chemical potential differences. The difference between the zinc blende and wurtzite structures can be described by the cohesive energy, so that $\mu_{AD}^{WZ} = \mu_{AD}^{ZB} + \psi_{AD}$ and $\mu_{BD}^{WZ} = \mu_{BD}^{ZB} + \psi_{BD}$. Finally, for calculation of the chemical potentials, the relation between the liquid and solid compositions is needed. For example, one may use the nucleation model which is described in *Paper I*.

The probability of the crystal phase formation in $\text{In}_x\text{Ga}_{1-x}\text{As}$ nanowires is a complicated function and depends on parameters of the liquid composition (and thus the solid composition), temperature, the contact angle, the WZ/ZB surface energy ratio and the Au concentration in the liquid particle. The following is the summary of the main trends from the theoretical analysis of the crystal structure formation of Au-catalyzed $\text{In}_x\text{Ga}_{1-x}\text{As}$ nanowires:

- (i) Nanowires tend to form in the cubic phase at high In content (close to InAs) and in the hexagonal phase at low In content (close to GaAs) (see Figure 2 in *Paper V*).
- (ii) With increasing temperature, the formation probability of the cubic phase increases (see Figure 2 in *Paper V*).
- (iii) With increasing the contact angle, the formation probability of the cubic phase increases (see Figure 3 in *Paper V*).
- (iv) The dependence of crystal structure formation on the Au concentration was found to be complex: nanowires tend to form in the cubic phase at low and high values of the Au concentration and in the hexagonal phase at intermediate ones (see Figure 4.6).

Such double transition has been experimentally observed in GaAs nanowires grown by MOVPE. In particular, it has been found that nanowires grew in the zincblende structure at low and very high V/III ratio while at high V/III ratio nanowires grew in the wurtzite structure [123], [124]. Unfortunately, the absolute values of the V/III ratio corresponding to zinc blende and wurtzite crystal structure vary from experiment to experiment which might be explained by different growth conditions. However, as shown in [121], the Ga content increases rapidly with increasing the TMGa flow at a certain V/III ratio. Thus, it seems that the gas phase (its composition and pressure) determines the composition of the liquid particles, which, in turn, determines the crystal phase. This gives rise to the use of the presented approach for description of the nanowire crystal structure. However, the transition is too rapid

because of the nucleation-limited composition. To fix it, one should substitute the liquid-solid composition dependence obtained within the incorporation model.

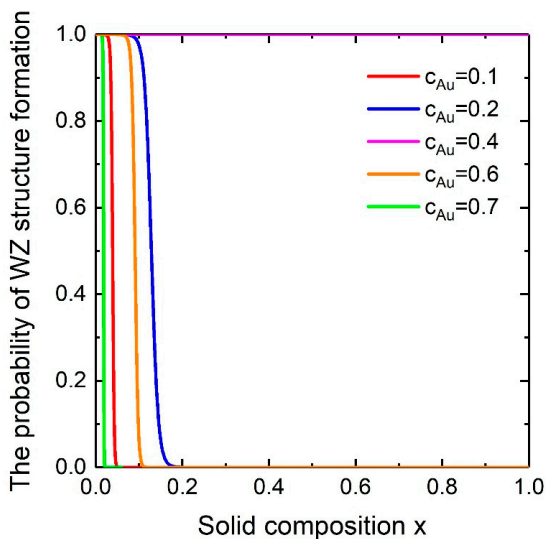


Figure 4.6. The probability of the hexagonal phase versus the solid composition in Au-catalyzed $\text{In}_x\text{Ga}_{1-x}\text{As}$ nanowires at different Au concentrations at fixed $\tau = 0.83$, $T = 550$ °C, $\beta = 110^\circ$, $c_{\text{As}} = 0.02$ and $R_{\text{NW}} = 100$ nm (the parameters are explained in *Paper V*).

Figure 3 in *Paper V* shows the probability of WZ structure formation as a function of the solid composition of Au-catalyzed $\text{In}_x\text{Ga}_{1-x}\text{As}$ nanowires calculated at different wetting angles. In other words, the difference is determined by the change of the effective surface energy Γ with the contact angle according to Eq. (29). However, the contact angle is not an arbitrary parameter. Within Au-catalyzed growth it should depend on the composition of the liquid particle, namely the III/Au ratio. Indeed, since Au atoms do not incorporate into the solid [125] and the As concentration is less than 1%, increase of the number of group III atoms in the liquid will change the droplet shape. Using the geometrical equations which link the nanowire radius and droplet volume, it is possible to estimate the content of group III atoms in the catalyst droplet if the number of Au atoms is known.

5 Summary and Outlook

To summarize, the composition and crystal structure of ternary nanowires nucleating from quaternary liquid melts have been studied by theoretical models.

The nanowire composition has been considered with two models, namely the nucleation and incorporation models. First, an analytic expression for the composition of a ternary III-V nanowire as a function of the liquid droplet composition has been derived. The core of the model is two-component heterogeneous nucleation. The distinguishing feature is that numerous interactions occurring during VLS growth from a quaternary liquid melt are considered, including the composition dependent interaction parameters. The In-Ga-As-Au, Al-Ga-As-Au, In-Ga-Sb-Au and In-Sb-As-Au materials systems have been considered and discussed in detail. It has been found that the composition of $\text{Al}_x\text{Ga}_{1-x}\text{As}$ can be varied over a wide range of the droplet composition. However, for several materials systems such as $\text{In}_x\text{Ga}_{1-x}\text{Sb}$ and $\text{In}_x\text{Ga}_{1-x}\text{As}$, composition tuning is limited by a large miscibility gap. The reason for the thermodynamically forbidden composition-range is a high value of the pseudobinary interaction parameter. In any case, composition tuning over a wide range requires a very high concentration ratio in the droplet. The comparison of the analytical expression with the numerical calculation showed the proximity of results. Then, we explained how the surface energy influences the miscibility gap during nucleation from a liquid melt. Within the second model, we studied the role of thermodynamics and kinetics in the formation of ternary III-V nanowires and simulated the evolution of the nucleus composition during vapor-liquid-solid growth.

Next, a model which allows us to describe ZB-WZ polytypism has been developed by introducing the difference in the cohesive energy between the ZB and WZ structures. To do so, the probabilities of nucleus formation of both ZB and WZ structures at the triple line or in the center of the growth interface have been calculated using the example of $\text{In}_x\text{Ga}_{1-x}\text{As}$ NWs. The obtained theoretical results agree with available experimental data.

To highlight, the novelty of the research is the following. First, the composition tuning in Au-catalyzed ternary III-V nanowire has been considered. Interaction parameters of any kind are considered. Second, the influence of the surface energy of a ternary nucleus on the liquid-solid composition dependence and the miscibility gap has been studied. Third, thermodynamic and kinetic approaches have been

combined given the opportunity to model the composition evolution in ternary nanowires during nucleation and monolayer completion. The proposed model allows us to describe the miscibility gap suppression at high supersaturation. Finally, the crystal structure of ternary nanowires has been theoretically studied.

All the models can be easily applied to other ternary III-V nanowires nucleating from quaternary melts. By doing this, the values of Gibbs free energies, interaction parameters and specific surface energies of the chosen material system should be substituted in the corresponding places. The foreign solvent U might be any element relevant as a catalyst or one can put its concentration to zero to describe self-catalyzed nanowires.

Some of the theoretical results have been experimentally verified by *in-situ* measurements. In particular, the incorporation model which takes into consideration the nucleus surface energy fits well the experimental liquid-solid composition dependence obtained during growth of $\text{In}_x\text{Ga}_{1-x}\text{As}$ nanowires in an environmental transmission electron microscope. One should remember that the nucleation model describes the formation of the critical nucleus, namely its composition and crystal structure. In general, the properties of the growing monolayer (and the nanowire) might differ from those of the critical nucleus. However, since the elongation rate of a nanowire is often limited by nucleation, the results might be used for the explanation of the growth rate.

The findings provide insights into nanowire growth and might be useful for optimization of the growth parameters. So, one can utilize the results to grow nanowires with a given composition or with a uniform crystal structure. This is important, since nanowires with controllable properties are necessary for the development of nanowire-based electronic and optoelectronic devices such as solar cells.

Despite of the fact that the thesis is devoted to nanowire growth modelling, there are no fundamental assumptions which would prevent the use of the presented models for description of other structures. So, for example one might use them for description of structures grown by liquid phase epitaxy.

There are several directions for future investigations in this topic. First, it is the thermodynamic assessment of the Gibbs free energies and interaction parameters of new ternary and quaternary materials systems. Then the obtained values can be used for nanowire growth modelling. Second, the thermodynamic model can be used for the modelling of heterostructure interfaces in nanowires. Third, finding a more accurate form for the difference in the cohesive energy between ZB and WZ is of great importance for the modelling crystal structure of NWs. One may apply the liquid-solid composition dependence obtained for the kinetic steady state regime to description of nanowire crystal structure. More smooth transition between the crystal phases is expected. Then, one could verify the model comparing the theoretical results with the experimental data on nanowire growth with mixed

crystal structure. Finally, one could consider size-dependent effects and quantum corrections to nucleation and growth models, namely to replace bulk phase diagrams with phase equilibria calculated for nano-systems.

References

1. Wagner, R.S. and Ellis, W.C. Vapor-Liquid-Solid Mechanism of Single Crystal Growth. *Applied Physics Letters* **1964**, 4, 89-90.
2. Sakaki, H. Scattering Suppression and High-Mobility Effect of Size-Quantized Electrons in Ultrafine Semiconductor Wire Structures. *Japanese Journal of Applied Physics* **1980**, 19, L735-L738.
3. Гиваргизов, Е.И., *Рост нитевидных и пластинчатых кристаллов из пара*. 1977: Москва : Наука. 303 с.
4. Wallentin, J.; Anttu, N.; Asoli, D.; Huffman, M.; Aberg, I.; Magnusson, M.H.; Siefert, G.; Fuss-Kailuweit, P.; Dimroth, F.; Witzigmann, B.; Xu, H.Q.; Samuelson, L.; Deppert, K., and Borgstrom, M.T. InP nanowire array solar cells achieving 13.8% efficiency by exceeding the ray optics limit. *Science* **2013**, 339, 1057-60.
5. Karimi, M.; Jain, V.; Heurlin, M.; Nowzari, A.; Hussain, L.; Lindgren, D.; Stehr, J.E.; Buyanova, I.A.; Gustafsson, A.; Samuelson, L.; Borgstrom, M.T., and Pettersson, H. Room-temperature InP/InAsP Quantum Discs-in-Nanowire Infrared Photodetectors. *Nano Lett* **2017**, 17, 3356-3362.
6. Patolsky, F.; Zheng, G.; Hayden, O.; Lakadamyali, M.; Zhuang, X., and Lieber, C.M. Electrical detection of single viruses. *Proc Natl Acad Sci U S A* **2004**, 101, 14017-22.
7. Zheng, G.; Lu, W.; Jin, S., and Lieber, C.M. Synthesis and Fabrication of High-Performance n-Type Silicon Nanowire Transistors. *Advanced Materials* **2004**, 16, 1890-1893.
8. Ross, F.M. Controlling nanowire structures through real time growth studies. *Reports on Progress in Physics* **2010**, 73, 114501.
9. Harmand, J.C.; Patriarche, G.; Glas, F.; Panciera, F.; Florea, I.; Maurice, J.L.; Travers, L., and Ollivier, Y. Atomic Step Flow on a Nanofacet. *Phys Rev Lett* **2018**, 121, 166101.
10. Jacobsson, D.; Panciera, F.; Tersoff, J.; Reuter, M.C.; Lehmann, S.; Hofmann, S.; Dick, K.A., and Ross, F.M. Interface dynamics and crystal phase switching in GaAs nanowires. *Nature* **2016**, 531, 317-22.
11. Stepanova, M. and Dew, S., *Nanofabrication*. Nanofabrication. 2012.
12. Guo, L.J. Nanoimprint Lithography: Methods and Material Requirements. *Advanced Materials* **2007**, 19, 495-513.
13. Manfrinato, V.R.; Zhang, L.; Su, D.; Duan, H.; Hobbs, R.G.; Stach, E.A., and Berggren, K.K. Resolution limits of electron-beam lithography toward the atomic scale. *Nano Lett* **2013**, 13, 1555-8.

14. Joyce, H.J., *III-V Nanowires and Related Nanostructures*, in *Metalorganic Vapor Phase Epitaxy (MOVPE)*. 2019. p. 217-239.
15. Redwing, J.M.; Miao, X., and Li, X., *Vapor-Liquid-Solid Growth of Semiconductor Nanowires*, in *Handbook of Crystal Growth: Thin Films and Epitaxy*. 2015, Elsevier Inc. p. 399-439.
16. Ohlsson, B.J.; Björk, M.T.; Magnusson, M.H.; Deppert, K.; Samuelson, L., and Wallenberg, L.R. Size-, shape-, and position-controlled GaAs nanowhiskers. *Applied Physics Letters* **2001**, *79*, 3335-3337.
17. Bemski, G. Recombination Properties of Gold in Silicon. *Physical Review* **1958**, *111*, 1515-1518.
18. Jansen, M.M.; Perla, P.; Kaladzhian, M.; von den Driesch, N.; Janßen, J.; Luysberg, M.; Lepsa, M.I.; Grützmacher, D., and Pawlis, A. Phase-Pure Wurtzite GaAs Nanowires Grown by Self-Catalyzed Selective Area Molecular Beam Epitaxy for Advanced Laser Devices and Quantum Disks. *ACS Applied Nano Materials* **2020**, *3*, 11037-11047.
19. Fontcuberta i Morral, A.; Colombo, C.; Abstreiter, G.; Arbiol, J., and Morante, J.R. Nucleation mechanism of gallium-assisted molecular beam epitaxy growth of gallium arsenide nanowires. *Applied Physics Letters* **2008**, *92*, 063112.
20. Dubrovskii, V.G. Kinetic narrowing of size distribution. *Physical Review B* **2016**, *93*, 174203.
21. Tersoff, J. Stable Self-Catalyzed Growth of III-V Nanowires. *Nano Lett* **2015**, *15*, 6609-13.
22. Leshchenko, E.D.; Turchina, M.A., and Dubrovskii, V.G. The initial stage of autocatalytic growth of GaAs filamentary nanocrystals. *Technical Physics Letters* **2016**, *42*, 818-821.
23. Persson, A.I.; Larsson, M.W.; Stenstrom, S.; Ohlsson, B.J.; Samuelson, L., and Wallenberg, L.R. Solid-phase diffusion mechanism for GaAs nanowire growth. *Nat Mater* **2004**, *3*, 677-81.
24. Heitsch, A.T.; Fanfair, D.D.; Tuan, H.Y., and Korgel, B.A. Solution-liquid-solid (SLS) growth of silicon nanowires. *J Am Chem Soc* **2008**, *130*, 5436-7.
25. Wang, F.; Dong, A., and Buhro, W.E. Solution-Liquid-Solid Synthesis, Properties, and Applications of One-Dimensional Colloidal Semiconductor Nanorods and Nanowires. *Chem Rev* **2016**, *116*, 10888-933.
26. Yuan, F.-W. and Tuan, H.-Y. Supercritical Fluid–Solid Growth of Single-Crystalline Silicon Nanowires: An Example of Metal-Free Growth in an Organic Solvent. *Crystal Growth & Design* **2010**, *10*, 4741-4745.
27. Tuan, H.-Y.; Lee, D.C.; Hanrath, T., and Korgel, B.A. Germanium Nanowire Synthesis: An Example of Solid-Phase Seeded Growth with Nickel Nanocrystals. *Chemistry of Materials* **2005**, *17*, 5705-5711.
28. Holmes, J.D.; Johnston, K.P.; Doty, R.C., and Korgel, B.A. Control of thickness and orientation of solution-grown silicon nanowires. *Science* **2000**, *287*, 1471-3.

29. Jabeen, F.; Rubini, S., and Martelli, F. Growth of III–V semiconductor nanowires by molecular beam epitaxy. *Microelectronics Journal* **2009**, *40*, 442-445.
30. Ikejiri, K.; Noborisaka, J.; Hara, S.; Motohisa, J., and Fukui, T. Mechanism of catalyst-free growth of GaAs nanowires by selective area MOVPE. *Journal of Crystal Growth* **2007**, *298*, 616-619.
31. Gil, E.; André, Y.; Cadoret, R., and Trassoudaine, A., *Hydride Vapor Phase Epitaxy for Current III–V and Nitride Semiconductor Compound Issues*, in *Handbook of Crystal Growth*. 2015. p. 51-93.
32. Heurlin, M.; Magnusson, M.H.; Lindgren, D.; Ek, M.; Wallenberg, L.R.; Deppert, K., and Samuelson, L. Continuous gas-phase synthesis of nanowires with tunable properties. *Nature* **2012**, *492*, 90-4.
33. Yuan, X.; Pan, D.; Zhou, Y.; Zhang, X.; Peng, K.; Zhao, B.; Deng, M.; He, J.; Tan, H.H., and Jagadish, C. Selective area epitaxy of III–V nanostructure arrays and networks: Growth, applications, and future directions. *Applied Physics Reviews* **2021**, *8*, 021302.
34. Kruse, J.E.; Lymperakis, L.; Eftychis, S.; Adikimenakis, A.; Doundoulakis, G.; Tsagaraki, K.; Androulidaki, M.; Olziersky, A.; Dimitrakis, P.; Ioannou-Sougleridis, V.; Normand, P.; Koukoula, T.; Kehagias, T.; Komninou, P.; Konstantinidis, G., and Georgakilas, A. Selective-area growth of GaN nanowires on SiO₂-masked Si (111) substrates by molecular beam epitaxy. *Journal of Applied Physics* **2016**, *119*, 224305.
35. Dubrovskii, V.G. Evolution of the Length and Radius of Catalyst-Free III-V Nanowires Grown by Selective Area Epitaxy. *ACS Omega* **2019**, *4*, 8400-8405.
36. Colson, P.; Henrist, C., and Cloots, R. Nanosphere Lithography: A Powerful Method for the Controlled Manufacturing of Nanomaterials. *Journal of Nanomaterials* **2013**, *2013*, 1-19.
37. Li, L.; Fang, Y.; Xu, C.; Zhao, Y.; Wu, K.; Limburg, C.; Jiang, P., and Ziegler, K.J. Controlling the Geometries of Si Nanowires through Tunable Nanosphere Lithography. *ACS Appl Mater Interfaces* **2017**, *9*, 7368-7375.
38. Cummins, C.; Ghoshal, T.; Holmes, J.D., and Morris, M.A. Strategies for Inorganic Incorporation using Neat Block Copolymer Thin Films for Etch Mask Function and Nanotechnological Application. *Adv Mater* **2016**, *28*, 5586-618.
39. Crossland, E.J.W.; Ludwigs, S.; Hillmyer, M.A., and Steiner, U. Freestanding nanowire arrays from soft-etch block copolymer templates. *Soft Matter* **2006**, *3*, 94-98.
40. Matsen, M.W. and Bates, F.S. Unifying Weak- and Strong-Segregation Block Copolymer Theories. *Macromolecules* **1996**, *29*, 1091-1098.
41. Thurn-Albrecht, T.; Schotter, J.; Kastle, G.A.; Emley, N.; Shibauchi, T.; Krusin-Elbaum, L.; Guarini, K.; Black, C.T.; Tuominen, M.T., and Russell, T.P. Ultrahigh-density nanowire arrays grown in self-assembled diblock copolymer templates. *Science* **2000**, *290*, 2126-9.

42. Dubrovskii, V.G., *Nucleation Theory and Growth of Nanostructures*. NanoScience and Technology. 2014.
43. Dubrovskii, V.G. Influence of the group V element on the chemical potential and crystal structure of Au-catalyzed III-V nanowires. *Applied Physics Letters* **2014**, 104, 053110.
44. Wang, H.; Zepeda-Ruiz, L.A.; Gilmer, G.H., and Upmanyu, M. Atomistics of vapour-liquid-solid nanowire growth. *Nat Commun* **2013**, 4, 1956.
45. Wang, B.; Yin, S.; Wang, G.; Buldum, A., and Zhao, J. Novel structures and properties of gold nanowires. *Phys Rev Lett* **2001**, 86, 2046-9.
46. Chen, W.; Dubrovskii, V.G.; Liu, X.; Xu, T.; Lardé, R.; Philippe Nys, J.; Grandidier, B.; Stiévenard, D.; Patriarche, G., and Pareige, P. Boron distribution in the core of Si nanowire grown by chemical vapor deposition. *Journal of Applied Physics* **2012**, 111, 094909.
47. Stringfellow, G.B. Calculation of ternary phase diagrams of III–V systems. *Journal of Physics and Chemistry of Solids* **1972**, 33, 665-677.
48. Lukas, H.; Fries, S.G., and Sundman, B., *Computational Thermodynamics*. 2007. 324.
49. Barin, I., *Thermochemical Data of Pure Substances*. 1995.
50. Okamoto, H. and Massalski, T.B. The Au–P (Gold-phosphorus) system. *Bulletin of Alloy Phase Diagrams* **1984**, 5, 490-491.
51. Davies, R.H.; Dinsdale, A.T.; Gisby, J.A.; Robinson, J.A.J., and Martin, S.M. MTDATA - thermodynamic and phase equilibrium software from the national physical laboratory. *Calphad* **2002**, 26, 229-271.
52. Andersson, J.O.; Helander, T.; Höglund, L.; Shi, P., and Sundman, B. Thermo-Calc & DICTRA, computational tools for materials science. *Calphad* **2002**, 26, 273-312.
53. Bale, C.W.; Chartrand, P.; Degterov, S.A.; Eriksson, G.; Hack, K.; Ben Mahfoud, R.; Melançon, J.; Pelton, A.D., and Petersen, S. FactSage thermochemical software and databases. *Calphad* **2002**, 26, 189-228.
54. Chen, S.L.; Daniel, S.; Zhang, F.; Chang, Y.A.; Yan, X.Y.; Xie, F.Y.; Schmid-Fetzer, R., and Oates, W.A. The PANDAT software package and its applications. *Calphad* **2002**, 26, 175-188.
55. Sundman, B.; Kattner, U.R.; Palumbo, M., and Fries, S.G. OpenCalphad - a free thermodynamic software. *Integrating Materials and Manufacturing Innovation* **2015**, 4, 1-15.
56. Glas, F.; Harmand, J.C., and Patriarche, G. Why does wurtzite form in nanowires of III-V zinc blende semiconductors? *Phys Rev Lett* **2007**, 99, 146101.
57. Akiyama, T.; Sano, K.; Nakamura, K., and Ito, T. An Empirical Potential Approach to Wurtzite-Zinc-Blende Polytypism in Group III-V Semiconductor Nanowires. *Japanese Journal of Applied Physics* **2006**, 45, L275-L278.
58. Dubrovskii, V.G. and Sibirev, N.V. Growth thermodynamics of nanowires and its application to polytypism of zinc blende III-V nanowires. *Physical Review B* **2008**, 77, 035414.

59. Vukajlovic-Plestina, J.; Kim, W.; Dubrovski, V.G.; Tutuncuoglu, G.; Lagier, M.; Potts, H.; Friedl, M., and Fontcuberta, I.M.A. Engineering the Size Distributions of Ordered GaAs Nanowires on Silicon. *Nano Lett* **2017**, 17, 4101-4108.
60. Dubrovskii, V.G.; Xu, T.; Alvarez, A.D.; Plissard, S.R.; Caroff, P.; Glas, F., and Grandidier, B. Self-Equilibration of the Diameter of Ga-Catalyzed GaAs Nanowires. *Nano Lett* **2015**, 15, 5580-4.
61. Dubrovskii, V.G.; Cirlin, G.E.; Soshnikov, I.P.; Tonkikh, A.A.; Sibirev, N.V.; Samsonenko, Y.B., and Ustinov, V.M. Diffusion-induced growth of GaAs nanowiskers during molecular beam epitaxy: Theory and experiment. *Physical Review B* **2005**, 71.
62. Kalache, B.; Cabarrocas, P.R.i., and Morral, A.F.i. Observation of Incubation Times in the Nucleation of Silicon Nanowires Obtained by the Vapor-Liquid-Solid Method. *Japanese Journal of Applied Physics* **2006**, 45, L190-L193.
63. Dubrovskii, V.G.; Sibirev, N.V.; Berdnikov, Y.; Gomes, U.P.; Ercolani, D.; Zannier, V., and Sorba, L. Length distributions of Au-catalyzed and In-catalyzed InAs nanowires. *Nanotechnology* **2016**, 27, 375602.
64. Koivusalo, E.S.; Hakkarainen, T.V.; Guina, M.D., and Dubrovskii, V.G. Sub-Poissonian Narrowing of Length Distributions Realized in Ga-Catalyzed GaAs Nanowires. *Nano Lett* **2017**, 17, 5350-5355.
65. Nagashima, K.; Yanagida, T.; Oka, K.; Tanaka, H., and Kawai, T. Mechanism and control of sidewall growth and catalyst diffusion on oxide nanowire vapor-liquid-solid growth. *Applied Physics Letters* **2008**, 93, 153103.
66. Ghasemi, M.; Leshchenko, E.D., and Johansson, J. Assembling your nanowire: an overview of composition tuning in ternary III-V nanowires. *Nanotechnology* **2021**, 32, 072001.
67. Liu, B.; Li, J.; Yang, W.; Zhang, X.; Jiang, X., and Bando, Y. Semiconductor Solid-Solution Nanostructures: Synthesis, Property Tailoring, and Applications. *Small* **2017**, 13, 1701998.
68. Ning, C.-Z.; Dou, L., and Yang, P. Bandgap engineering in semiconductor alloy nanomaterials with widely tunable compositions. *Nature Reviews Materials* **2017**, 2, 17070.
69. Barrigon, E.; Heurlin, M.; Bi, Z.; Monemar, B., and Samuelson, L. Synthesis and Applications of III-V Nanowires. *Chem Rev* **2019**, 119, 9170-9220.
70. Li, Y.; Weatherly †, G.C., and Niewczas *, M. TEM studies of stress relaxation in GaAsN and GaP thin films. *Philosophical Magazine* **2005**, 85, 3073-3090.
71. Luryi, S. and Suhir, E. New approach to the high quality epitaxial growth of lattice-mismatched materials. *Applied Physics Letters* **1986**, 49, 140-142.
72. Zubia, D. and Hersee, S.D. Nanoheteroepitaxy: The Application of nanostructuring and substrate compliance to the heteroepitaxy of mismatched semiconductor materials. *Journal of Applied Physics* **1999**, 85, 6492-6496.
73. Glas, F. Critical dimensions for the plastic relaxation of strained axial heterostructures in free-standing nanowires. *Physical Review B* **2006**, 74, 121302(R).

74. Borg, B.M.; Dick, K.A.; Eymery, J., and Wernersson, L.-E. Enhanced Sb incorporation in InAsSb nanowires grown by metalorganic vapor phase epitaxy. *Applied Physics Letters* **2011**, 98, 113104.
75. Wu, J.; Borg, B.M.; Jacobsson, D.; Dick, K.A., and Wernersson, L.-E. Control of composition and morphology in InGaAs nanowires grown by metalorganic vapor phase epitaxy. *Journal of Crystal Growth* **2013**, 383, 158-165.
76. DeHoff, R., *Thermodynamics in Materials Science*. 2006.
77. Roche, E.; Andre, Y.; Avit, G.; Bougerol, C.; Castelluci, D.; Reveret, F.; Gil, E.; Medard, F.; Leymarie, J.; Jean, T.; Dubrovskii, V.G., and Trassoudaine, A. Circumventing the miscibility gap in InGaN nanowires emitting from blue to red. *Nanotechnology* **2018**, 29, 465602.
78. Glas, F. Comparison of Modeling Strategies for the Growth of Heterostructures in III–V Nanowires. *Crystal Growth & Design* **2017**, 17, 4785-4794.
79. Li, N.; Tan, T.Y., and Gösele, U. Transition region width of nanowire hetero- and pn-junctions grown using vapor–liquid–solid processes. *Applied Physics A* **2008**, 90, 591-596.
80. Paladugu, M.; Zou, J.; Guo, Y.-N.; Zhang, X.; Kim, Y.; Joyce, H.J.; Gao, Q.; Tan, H.H., and Jagadish, C. Nature of heterointerfaces in GaAs/InAs and InAs/GaAs axial nanowire heterostructures. *Applied Physics Letters* **2008**, 93, 101911.
81. Dick, K.A.; Bolinsson, J.; Borg, B.M., and Johansson, J. Controlling the abruptness of axial heterojunctions in III-V nanowires: beyond the reservoir effect. *Nano Lett* **2012**, 12, 3200-6.
82. Zannier, V.; Rossi, F.; Dubrovskii, V.G.; Ercolani, D.; Battiato, S., and Sorba, L. Nanoparticle Stability in Axial InAs-InP Nanowire Heterostructures with Atomically Sharp Interfaces. *Nano Lett* **2018**, 18, 167-174.
83. Dastjerdi, M.H.T.; Fiordaliso, E.M.; Leshchenko, E.D.; Akhtari-Zavareh, A.; Kasama, T.; Aagesen, M.; Dubrovskii, V.G., and LaPierre, R.R. Three-fold Symmetric Doping Mechanism in GaAs Nanowires. *Nano Lett* **2017**, 17, 5875-5882.
84. Hakkarainen, T.; Piton, M.R.; Fiordaliso, E.M.; Leshchenko, E.D.; Koelling, S.; Bettini, J.; Galetti, H.V.A.; Koivusalo, E.; Gobato, Y.G.; Rodrigues, A.D.; Lupo, D.; Koenraad, P.M.; Leite, E.R.; Dubrovskii, V.G., and Guina, M. Te incorporation and activation as n-type dopant in self-catalyzed GaAs nanowires. *Physical Review Materials* **2019**, 3, 086001.
85. Dick, K.A.; Caroff, P.; Bolinsson, J.; Messing, M.E.; Johansson, J.; Deppert, K.; Wallenberg, L.R., and Samuelson, L. Control of III–V nanowire crystal structure by growth parameter tuning. *Semiconductor Science and Technology* **2010**, 25, 024009.
86. Caroff, P.; Dick, K.A.; Johansson, J.; Messing, M.E.; Deppert, K., and Samuelson, L. Controlled polytypic and twin-plane superlattices in iii-v nanowires. *Nat Nanotechnol* **2009**, 4, 50-5.

87. Ameruddin, A.S.; Fonseka, H.A.; Caroff, P.; Wong-Leung, J.; Op het Veld, R.L.; Boland, J.L.; Johnston, M.B.; Tan, H.H., and Jagadish, C. In(x)Ga(1-x)As nanowires with uniform composition, pure wurtzite crystal phase and taper-free morphology. *Nanotechnology* **2015**, 26, 205604.
88. Dick, K.A.; Thelander, C.; Samuelson, L., and Caroff, P. Crystal phase engineering in single InAs nanowires. *Nano Lett* **2010**, 10, 3494-9.
89. Bauer, B.; Rudolph, A.; Soda, M.; Fontcuberta i Morral, A.; Zweck, J.; Schuh, D., and Reiger, E. Position controlled self-catalyzed growth of GaAs nanowires by molecular beam epitaxy. *Nanotechnology* **2010**, 21, 435601.
90. Leshchenko, E.D.; Kuyanov, P.; LaPierre, R.R., and Dubrovskii, V.G. Tuning the morphology of self-assisted GaP nanowires. *Nanotechnology* **2018**, 29, 225603.
91. Borgstrom, M.T.; Immink, G.; Ketelaars, B.; Algra, R., and Bakkers, E.P. Synergetic nanowire growth. *Nat Nanotechnol* **2007**, 2, 541-4.
92. Sibirev, N.V.; Tchernycheva, M.; Timofeeva, M.A.; Harmand, J.-C.; Cirlin, G.E., and Dubrovskii, V.G. Influence of shadow effect on the growth and shape of InAs nanowires. *Journal of Applied Physics* **2012**, 111, 104317.
93. Messing, M.E.; Hillerich, K.; Johansson, J.; Deppert, K., and Dick, K.A. The use of gold for fabrication of nanowire structures. *Gold Bulletin* **2009**, 42, 172-181.
94. Priante, G.; Glas, F.; Patriarche, G.; Pantzas, K.; Oehler, F., and Harmand, J.C. Sharpening the Interfaces of Axial Heterostructures in Self-Catalyzed AlGaAs Nanowires: Experiment and Theory. *Nano Lett* **2016**, 16, 1917-24.
95. Jung, C.S.; Kim, H.S.; Jung, G.B.; Gong, K.J.; Cho, Y.J.; Jang, S.Y.; Kim, C.H.; Lee, C.-W., and Park, J. Composition and Phase Tuned InGaAs Alloy Nanowires. *The Journal of Physical Chemistry C* **2011**, 115, 7843-7850.
96. Li, L.; Pan, D.; Xue, Y.; Wang, X.; Lin, M.; Su, D.; Zhang, Q.; Yu, X.; So, H.; Wei, D.; Sun, B.; Tan, P.; Pan, A., and Zhao, J. Near Full-Composition-Range High-Quality GaAs_{1-x}Sb_x Nanowires Grown by Molecular-Beam Epitaxy. *Nano Lett* **2017**, 17, 622-630.
97. Vegard, L. Die Konstitution der Mischkristalle und die Raumfüllung der Atome. *Zeitschrift für Physik* **1921**, 5, 17-26.
98. Stringfellow, G.B., *Organometallic Vapor-Phase Epitaxy*. 1999.
99. Tchernycheva, M.; Travers, L.; Patriarche, G.; Glas, F.; Harmand, J.-C.; Cirlin, G.E., and Dubrovskii, V.G. Au-assisted molecular beam epitaxy of InAs nanowires: Growth and theoretical analysis. *Journal of Applied Physics* **2007**, 102, 094313.
100. Dick, K.A.; Deppert, K.; Martensson, T.; Mandl, B.; Samuelson, L., and Seifert, W. Failure of the vapor-liquid-solid mechanism in Au-assisted MOVPE growth of InAs nanowires. *Nano Lett* **2005**, 5, 761-4.
101. Vukajlovic-Plestina, J.; Dubrovskii, V.G.; Tutuncuoglu, G.; Potts, H.; Ricca, R.; Meyer, F.; Matteini, F.; Leran, J.B., and AF, I.M. Molecular beam epitaxy of InAs nanowires in SiO₂ nanotube templates: challenges and prospects for integration of III-Vs on Si. *Nanotechnology* **2016**, 27, 455601.

102. Johansson, J. and Ghasemi, M. Kinetically limited composition of ternary III-V nanowires. *Physical Review Materials* **2017**, 1, 040401.
103. Dubrovskii, V.G.; Koryakin, A.A., and Sibirev, N.V. Understanding the composition of ternary III-V nanowires and axial nanowire heterostructures in nucleation-limited regime. *Materials & Design* **2017**, 132, 400-408.
104. Glas, F.; Ramdani, M.R.; Patriarche, G., and Harmand, J.-C. Predictive modeling of self-catalyzed III-V nanowire growth. *Physical Review B* **2013**, 88, 195304.
105. Ghahamestani, S.G.; Ek, M.; Ghasemi, M.; Caroff, P.; Johansson, J., and Dick, K.A. Morphology and composition controlled Ga(x)In(1-x)Sb nanowires: understanding ternary antimonide growth. *Nanoscale* **2014**, 6, 1086-92.
106. Dubrovskii, V.G. Fully Analytical Description for the Composition of Ternary Vapor-Liquid-Solid Nanowires. *Crystal Growth & Design* **2015**, 15, 5738-5743.
107. Yeh, C.Y.; Lu, Z.W.; Froyen, S., and Zunger, A. Zinc-blende-wurtzite polytypism in semiconductors. *Phys Rev B Condens Matter* **1992**, 46, 10086-10097.
108. Algra, R.E.; Verheijen, M.A.; Borgstrom, M.T.; Feiner, L.F.; Immink, G.; van Enckevort, W.J.; Vlieg, E., and Bakkers, E.P. Twinning superlattices in indium phosphide nanowires. *Nature* **2008**, 456, 369-72.
109. Dubrovskii, V.G.; Sibirev, N.V.; Harmand, J.C., and Glas, F. Growth kinetics and crystal structure of semiconductor nanowires. *Physical Review B* **2008**, 78, 235301.
110. Sosso, G.C.; Chen, J.; Cox, S.J.; Fitzner, M.; Pedevilla, P.; Zen, A., and Michaelides, A. Crystal Nucleation in Liquids: Open Questions and Future Challenges in Molecular Dynamics Simulations. *Chem Rev* **2016**, 116, 7078-116.
111. Laaksonen, A. and Napari, I. Breakdown of the Capillarity Approximation in Binary Nucleation: A Density Functional Study†. *The Journal of Physical Chemistry B* **2001**, 105, 11678-11682.
112. Lutsko, J.F. and Duran-Olivencia, M.A. Classical nucleation theory from a dynamical approach to nucleation. *J Chem Phys* **2013**, 138, 244908.
113. Kashchiev, D. Toward a better description of the nucleation rate of crystals and crystalline monolayers. *J Chem Phys* **2008**, 129, 164701.
114. Karthika, S.; Radhakrishnan, T.K., and Kalaichelvi, P. A Review of Classical and Nonclassical Nucleation Theories. *Crystal Growth & Design* **2016**, 16, 6663-6681.
115. Kalikmanov, V.I. Binary nucleation beyond capillarity approximation. *Phys Rev E Stat Nonlin Soft Matter Phys* **2010**, 81, 050601.
116. Dubrovskii, V.G.; Sibirev, N.V.; Cirlin, G.E.; Soshnikov, I.P.; Chen, W.H.; Larde, R.; Cadel, E.; Pareige, P.; Xu, T.; Grandidier, B.; Nys, J.P.; Stievenard, D.; Moewe, M.; Chuang, L.C., and Chang-Hasnain, C. Gibbs-Thomson and diffusion-induced contributions to the growth rate of Si, InP, and GaAs nanowires. *Physical Review B* **2009**, 79, 205316.

117. Connell, J.G.; Yoon, K.; Perea, D.E.; Schwalbach, E.J.; Voorhees, P.W., and Lauhon, L.J. Identification of an intrinsic source of doping inhomogeneity in vapor-liquid-solid-grown nanowires. *Nano Lett* **2013**, 13, 199-206.
118. Glas, F.; Harmand, J.C., and Patriarche, G. Nucleation antibunching in catalyst-assisted nanowire growth. *Phys Rev Lett* **2010**, 104, 135501.
119. Dubrovskii, V.G. and Grechenkov, J. Zeldovich Nucleation Rate, Self-Consistency Renormalization, and Crystal Phase of Au-Catalyzed GaAs Nanowires. *Crystal Growth & Design* **2014**, 15, 340-347.
120. Wilemski, G. Revised classical binary nucleation theory for aqueous alcohol and acetone vapors. *The Journal of Physical Chemistry* **1987**, 91, 2492-2498.
121. Maliakkal, C.B.; Jacobsson, D.; Tornberg, M.; Persson, A.R.; Johansson, J.; Wallenberg, R., and Dick, K.A. In situ analysis of catalyst composition during gold catalyzed GaAs nanowire growth. *Nat Commun* **2019**, 10, 4577.
122. Maliakkal, C.B.; Martensson, E.K.; Tornberg, M.U.; Jacobsson, D.; Persson, A.R.; Johansson, J.; Wallenberg, L.R., and Dick, K.A. Independent Control of Nucleation and Layer Growth in Nanowires. *ACS Nano* **2020**, 14, 3868-3875.
123. Lehmann, S.; Jacobsson, D., and Dick, K.A. Crystal phase control in GaAs nanowires: opposing trends in the Ga- and As-limited growth regimes. *Nanotechnology* **2015**, 26, 301001.
124. Martensson, E.K.; Lehmann, S.; Dick, K.A., and Johansson, J. Simulation of GaAs Nanowire Growth and Crystal Structure. *Nano Lett* **2019**, 19, 1197-1203.
125. Persson, A.R.; Tornberg, M.; Sjkqvist, R., and Jacobsson, D. Time-resolved compositional mapping during in situ TEM studies. *Ultramicroscopy* **2021**, 222, 113193.